



Epigallocatechin-3-gallate pretreatment alleviates doxorubicin-induced ferroptosis and cardiotoxicity by upregulating AMPK α 2 and activating adaptive autophagy

Huan He^{a,c}, Liang Wang^b, Yang Qiao^c, Bin Yang^c, Dong Yin^{d,**}, Ming He^{a,c,*}

^a Institute of Cardiovascular Diseases, Jiangxi Academy of Clinical Medical Sciences, The First Affiliated Hospital of Nanchang University, Nanchang, 330006, China

^b Department of Rehabilitation, The First Affiliated Hospital of Nanchang University, Nanchang, 330006, China

^c Jiangxi Provincial Key Laboratory of Basic Pharmacology, Nanchang University School of Pharmaceutical Science, Nanchang, 330006, China

^d Jiangxi Provincial Key Laboratory of Molecular Medicine, The Second Affiliated Hospital, Nanchang University, Nanchang, 330006, China

ARTICLE INFO

Keywords:

AMP-Activated protein kinase α 2
Autophagy
Cardiotoxicity
Doxorubicin
Epigallocatechin-3-gallate
Ferroptosis

ABSTRACT

Reports indicate that the mechanism of doxorubicin (Dox)-induced cardiotoxicity is very complex, involving multiple regulatory cell death forms. Furthermore, the clinical intervention effect is not ideal. Iron dependence, abnormal lipid metabolism, and excess reactive oxygen species generation, three characteristics of ferroptosis, are potential therapeutic intervention targets. Here, we confirmed in vitro and in vivo that at least autophagy, apoptosis, and ferroptosis are involved in Dox cardiotoxicity-induced damage. When the neonatal rat cardiomyocytes and H9C2 cells or C57BL/6 mice were subjected to Dox-induced cardiotoxicity, epigallocatechin-3-gallate pretreatment could effectively decrease iron accumulation, inhibit oxidative stress and abnormal lipid metabolism, and thereby alleviate Dox cardiotoxicity-induced ferroptosis and protect the myocardium according to multiple functional, enzymatic, and morphological indices. The underlying mechanism was verified to involve the upregulation and activation of AMP-activated protein kinase α 2, which promoted adaptive autophagy, increased energy supply, and maintained mitochondrial function. We believe that epigallocatechin-3-gallate is a candidate phytochemical against Dox-induced cardiotoxicity.

1. Introduction

Numerous clinical trials have confirmed that science-based and rational drug treatment can significantly reduce the mortality of patients with malignant tumors [1]. However, many chemotherapeutic agents are associated with adverse reactions, among which cardiotoxicity is the most common and poses direct threat to patients' life [2]. Anthracycline is widely used in chemotherapy for lymphoma, sarcoma, and breast cancer [3]. As the most commonly used anthracycline, doxorubicin (Dox) possesses strong anticancer activity, broad anticancer spectrum, and definite curative effect. However, its clinical application has been greatly limited because as many as one fourth of patients have experienced Dox-induced cardiotoxicity (DIC) [4]. Previous studies on the mechanism of DIC mainly focused on excess intracellular reactive oxygen species (ROS) generation, secondary to downstream protein, lipid, and DNA damage [5]. Several efforts have been devoted to the use of

drugs that decrease ROS generation. Still, the results of these efforts are not ideal, indicating that either the underlying mechanism is not only related to the oxidative stress originally proposed or that the exact mechanism is still unknown [6,7].

Recently, many studies have confirmed that Dox induces cardiomyocyte death through both accidental cell death or regulated cell death (RCD) mechanisms. The latter includes necroptosis, pyroptosis, autophagy, ferroptosis, and apoptosis, which occur simultaneously, and not independently, and overlap and crosstalk with each other, which greatly increases the complexity of DIC [8–10]. Furthermore, our previous works have found that apoptosis is involved in DIC and Dox-induced endotheliotoxicity, which could be intervened using certain phytochemicals [11–15]. At present, whether Dox induces or inhibits autophagy in the myocardium remains controversial [16–18]. However, recent studies have confirmed that ferroptosis plays a crucial role in DIC [19–21]. Ferroptosis is an iron- and lipotoxicity-dependent

* Corresponding author. No. 461, Bayi Road, 330006, Nanchang, China.

** Corresponding author. No. 1, Minde Road, 330006, Nanchang, China.

E-mail addresses: dongyin24@126.com (D. Yin), jxhm56@hotmail.com (M. He).

<https://doi.org/10.1016/j.redox.2021.102185>

Received 29 September 2021; Received in revised form 8 November 2021; Accepted 9 November 2021

Available online 11 November 2021

2213-2317/© 2021 The Authors.

Published by Elsevier B.V. This is an open access article under the CC BY-NC-ND license

(<http://creativecommons.org/licenses/by-nc-nd/4.0/>).

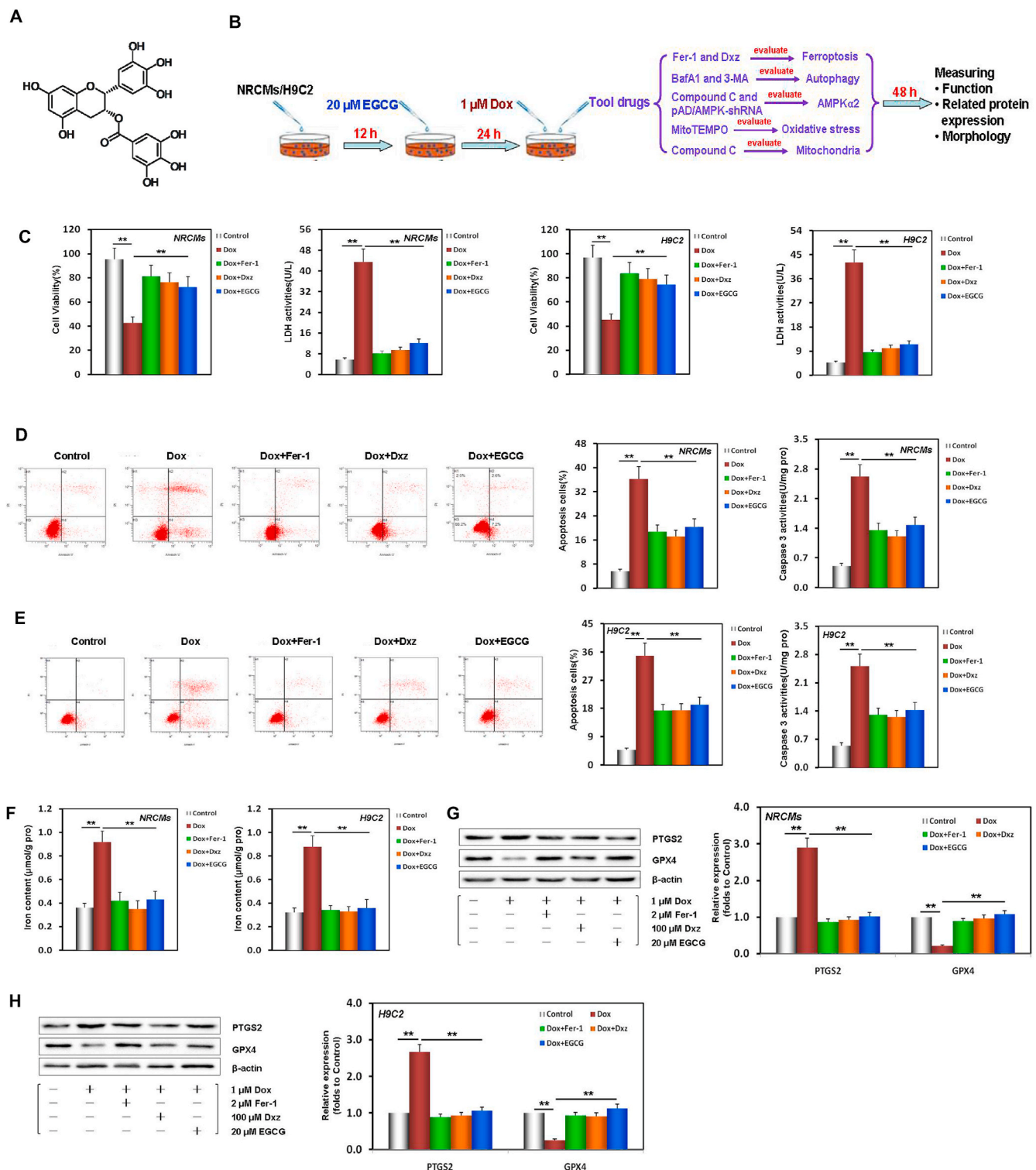


Fig. 1. EGCG pretreatment alleviated Dox-induced cardiomyocyte ferroptosis. **A** EGCG molecular formula. **B** Diagram of the in vitro study design. **C** NRCM and H9C2 cell viability and LDH activity (containing 20 μ M EGCG [during the 12 h pretreatment before exposure to 1 μ M Dox] in cells subjected to or not to 20 μ M EGCG, 2 μ M Fer-1, and 100 μ M Dxz co-treatment for 48 h; the below findings were also obtained using this method). **D** Apoptosis and caspase-3 activity of NRCMs. **E** Apoptosis and caspase-3 activity of H9C2 cells. **F** Iron contents of NRCMs and H9C2 cells. Values are mean \pm SD from five individual experiments. $^{**}p < 0.01$ compared with the indicated groups. **G** Western blot bands showing PTGS2 and GPX4 protein expression and the relative signal intensities in NRCMs. **H** Western blot bands showing PTGS2 and GPX4 protein expression and the relative signal intensities in H9C2 cells. **I** Transmission electron microscope images and the relative Fiameng scores of NRCMs. **J** Western blot bands showing LC3 and P62 protein expression and the relative signal intensities in NRCMs. **K** Western blot bands showing LC3 and P62 protein expression and the relative signal intensities in H9C2 cells. Values are mean \pm SD from three individual experiments. NS, nonsignificant. $^{*}p < 0.05$ compared with the indicated groups. $^{**}p < 0.01$ compared with the indicated groups.

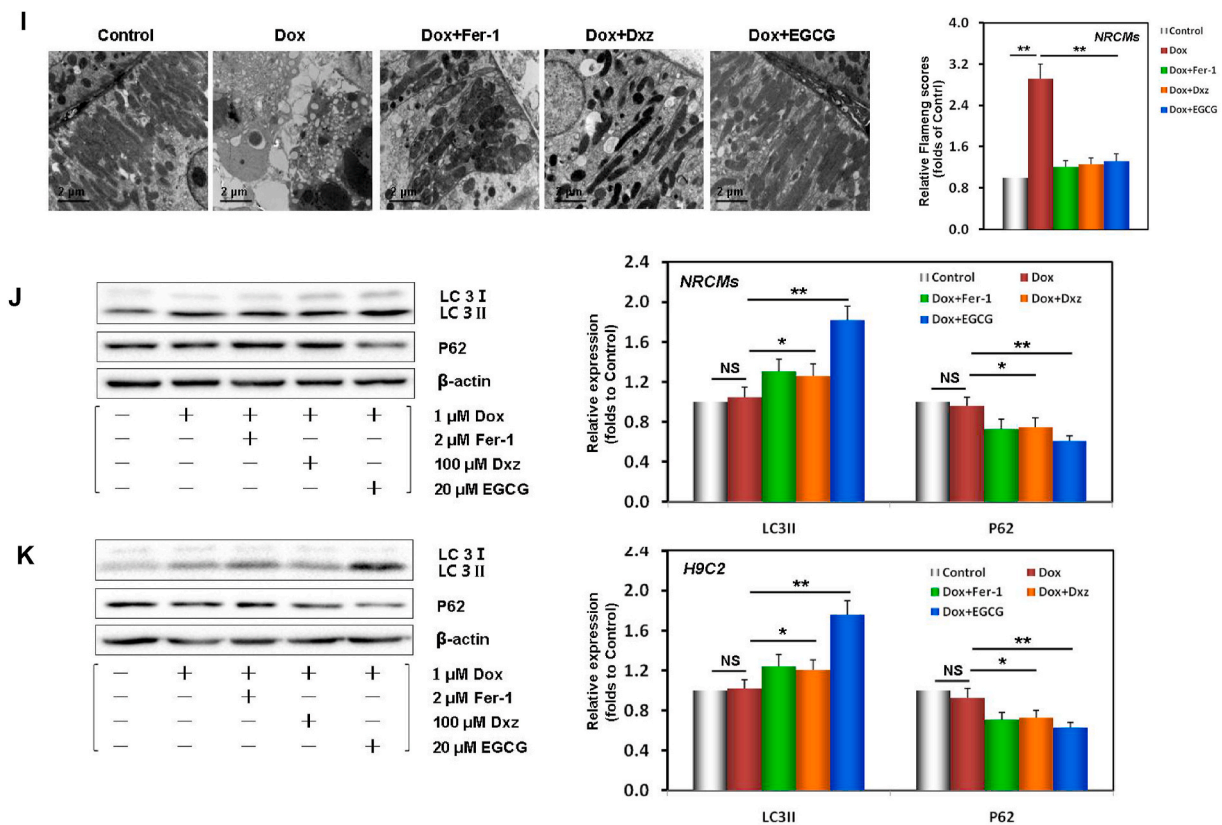


Fig. 1. (continued).

RCD [8–10,22]. Whether it occurs or not depends on the balance between ROS generation induced by iron accumulation and the antioxidant system that counteracts lipid peroxidation. On the other hand, iron dependence, abnormal lipid metabolism, and excess ROS generation, three characteristics of ferroptosis, are also likely to be good intervention targets [22,23]. Exploring the mechanism of DIC may help to identify new therapeutic targets and develop more targeted drugs.

(–)Epigallocatechin-3-gallate (EGCG, Fig. 1A), an active polyphenol compound derived from green tea, possesses multiple biological activities, such as antitumor, antibacterial, antiinflammatory, antiarteriosclerosis, and cytoprotective activities and is involved in the maintenance of mitochondrial function through multiple targets and mechanisms by changing the expression of some proteins (Nrf-2, ET-1, HO1, NADPH and Bcl-2) and cytokines and regulating ROS/ERK/JNK-p53, ADMA/DDAH/NOS/NO and PI-3K/AKT/NF-κB pathway [24,25]. EGCG has strong antioxidant activity and chelates divalent metal ions, such as iron, owing to its special stereochemical structure [26,27]. Studies found that EGCG could regulate the expression of specific active proteins, such as AMP-activated protein kinase (AMPK), and the corresponding signaling pathways, and intervene with cell autophagy and apoptosis [28–30]. Furthermore, some studies showed that EGCG could protect cardiomyocytes against DIC through anti-apoptotic mechanisms [31–33]. Recent reports revealed that EGCG protected mouse intestinal epithelial cells and alleviated ionizing radiation-induced ferroptosis [34], iron overload and erastin-induced pancreatic cell ferroptosis [35]. Furthermore, it was found to promote PKD1 phosphorylation and inhibit ferroptosis after spinal cord injury [36].

This study elucidated a new mechanism underlying the protective effect of EGCG pretreatment against DIC for the first time. We found that EGCG pretreatment could upregulate the expression and phosphorylation of AMPKα2 and activate adaptive autophagy, protecting the myocardium against ferroptosis associated with DIC.

2. Materials and methods

2.1. Animals and cells

Specific pathogen free (SPF) 8-week-old male C57BL/6 mice and neonatal (0–3 day) Sprague Dawley rats were obtained from the Animal Center of Nanchang University (Nanchang, China). All animal procedures abided by the National Institutes of Health (USA) guidelines and were authorized by the ethics committee of Nanchang University (No. 2020-0182). The mice were housed at 24 ± 1 °C, 50% humidity, and 12 h dark/light cycle, with regular provision of food and water.

The H9C2 cell line was obtained from the Cell Bank of the Chinese Academy of Sciences (Shanghai, China). Cells were cultured in Dulbecco's modified Eagle's medium (DMEM, Gibco-BRL, 11054001) with 10% fetal bovine serum (FBS, Gibco-BRL, 10099141) and 1% penicillin-streptomycin (Gibco-BRL, 15070063) in a humidified atmosphere at 37 °C and 5% CO₂.

2.2. Reagents and antibodies

EGCG (PHL89656), Dox (D1515), ferrostatin-1 (Fer-1, S7243), dexrazoxane (Dxz, 05587), 3-methyladenine (3-MA, S2767), A769662 (SML2578), MitoTEMPO (SML0737), compound C (P5499), bromodeoxyuridine (BrdU, B5002), and bafilomycin A1 (BafA1, S1413) were purchased from Sigma-Aldrich. Primary antibodies against NADH-ubiquinone oxidoreductase subunit B8 (NDUFB8, ab110242), ubiquinol-cytochrome c reductase core protein 2 (UQCRC2, ab203832), AMPKα2 (ab97275), p-AMPKα2 (S173, ab55886), acetyl-CoA carboxylase (ACC, ab45174), and p-ACC (S79, ab68919) were obtained from Abcam. Primary antibodies against prostaglandin-endoperoxide synthase 2 (PTGS2, 12282), glutathione peroxidase 4 (GPX4, 52455), microtubule-associated protein 1A/1B-light chain 3 (LC3-I/II, 43566), P62 (23214), mammalian target of rapamycin (mTOR, 2983), p-mTOR

(S2448, 5536), unc-51 like autophagy activating kinase 1 (ULK1, 8054), p-ULK1 (S757, 14202), GAPDH (2118), β -actin (3700), anti-rabbit IgG (7054), and anti-mouse IgG (7076) were purchased from Cell Signaling Technology. Adenovirus vector expressing short hairpin RNA targeting AMPK (pAD/AMPK-shRNA) was purchased from Gene Chem Co., Ltd.

2.3. NRCM isolation and culture

Neonatal rat cardiomyocytes (NRCMs) were isolated from the neonatal rat heart according to our previous reports [37,38]. Briefly, the ventricular muscles of neonatal rats were isolated quickly, digested repeatedly with 0.1% trypsin, and the cells were harvested. Non-myocyte was removed by differential adhesion method to obtain pure NRCMs. The NRCMs were resuspended with 80% DMEM (Gibco-BRL), 20% FBS (Gibco-BRL), 100 U/ml penicillin and streptomycin (Gibco-BRL), and 1% BrdU medium, and cultured in 95% O₂ and 5% CO₂ standard incubator at 37 °C.

2.4. Experimental design

2.4.1. In vitro experiments (Fig. 1B)

Firstly, to confirm that EGCG pretreatment could alleviate ferroptosis and protect cardiomyocytes against Dox toxicity, NRCMs and H9C2 cells were separated into five groups: 1) Dox, 2) Fer-1, 3) Dxz, 4) EGCG, and 5) control. The Dox group cells were incubated with normal medium for 24 h, and then exposed to 1 μ M Dox for 48 h [15]. The Fer-1 and Dxz group cells were incubated with normal medium for 24 h, and then co-treated with 2 μ M Fer-1 or 100 μ M Dxz and 1 μ M Dox for 48 h [19]. The EGCG group cells were pretreated with 20 μ M EGCG (dissolved in culture medium) for 24 h, and then co-treated with 1 μ M Dox for 48 h. The control group cells were incubated with normal medium for 72 h. Cell viability; lactate dehydrogenase (LDH) and caspase-3 activity; apoptosis; iron content; the expression of PTGS2, GPX4, LC3, and P62 in the lysate of NRCMs and H9C2 cells; and mitochondrial ultrastructure in NRCMs were assayed after the above processing.

Secondly, the alteration of autophagy under DIC damage and the influence of EGCG on the alteration were evaluated. NRCMs and H9C2 cells were co-treated using the autophagy inhibitor BafA1 (100 nM) [38] and 1 μ M Dox for 48 h. LC3 and P62 expression was assayed. Then, cells in the control, Dox, and EGCG groups were treated according to the above method. Cells in the 3-MA group were co-treated with 5 mM 3-MA [39], at the same time as 1 μ M Dox was added to the EGCG group. The expression levels of LC3 and P62, and the autolysosome content [38] were assayed again with the above treatment.

Thirdly, to explore if the AMPK α 2/mTOR/ULK1 pathway is participated in the pathophysiological process of activating autophagy under DIC injury and the role of EGCG pretreatment, NRCMs and H9C2 cells in the control, Dox, and EGCG groups were treated according to the above method. The compound C group NRCMs were co-treated with 5 μ M compound C [38], at the same time as 1 μ M Dox was added to the EGCG-treated group. The pAD/AMPK-shRNA group H9C2 cells were transfected using pAD/AMPK-shRNA at the same time as 1 μ M Dox was added to the EGCG-treated group. The expression and phosphorylation of AMPK α 2, mTOR, ULK1, and ACC, and the contents of α -Ketoglutarate (α -KG) and succinate (Suc) were determined after the above processing.

Additionally, we studied how EGCG pretreatment could prevent the damage of intracellular lipid metabolism and redox equilibrium caused by Dox-induced toxicity. Briefly, H9C2 cells in the control, Dox, Fer-1, and EGCG group were treated according to the above method. H9C2 cells in the MitoTEMPO group were co-treated with 10 μ M MitoTEMPO [40] and 1 μ M Dox for 48 h. Intracellular/mitochondrial ROS, the content of malonaldehyde (MDA) and 4-hydroxynonenal (4-HNE), the levels of glutathione (GSH) and glutathione disulfide (GSSG), and the GSH/GSSG ratio in H9C2 cells were determined after the above processing.

Finally, we investigated how EGCG pretreatment could maintain and

improve energy metabolism and mitochondrial function in NRCMs injured by Dox-induced toxicity. NRCMs in the control, Dox, EGCG, and compound C groups were treated according to the above method. The oxygen consumption rate (OCR) and extracellular acidification rate (ECAR), the expression of NDUFB8 and UQCRC2, the activities of complexes I and III in the electron transport chain (ETC) of mitochondrion, and mitochondrial membrane potential (MMP) levels in NRCMs were determined after the above processing.

2.4.2. In vivo experiments (Fig. 6A)

Mice were re-separated into 5 groups: control, Dox, Dox + Fer-1, Dox + EGCG, and Dox + EGCG + compound C groups. The Dox group mice were administered 6 intraperitoneal (ip) injections of 2.5 mg/kg Dox over 3 weeks for a cumulative dose of 15 mg/kg [15]. Mice in the Dox + Fer-1 group were ip injected with 1 mg/kg/d Fer-1 [19] for 2 weeks as in the Dox group. Mice in the Dox + EGCG group were intragastrically (ig) injected 20 mg/kg/d EGCG (dissolved in normal saline) for six consecutive weeks; Dox was administered 1 h prior to this as in the Dox group. Mice in the Dox + EGCG + compound C group were treated using the same method as in the Dox + EGCG group for four consecutive weeks, followed by ip injections of 10 mg/kg/d compound C [41] for 2 weeks. Mice in the control groups were administered an equal volume of normal saline via gavage for 6 weeks. Among them, the tool drugs were given by intraperitoneal injection (ip) as required. Considering future transformation applications, EGCG was administered orally (ig).

Twenty-four hours after the last ig injection of EGCG, mice were anesthetized using ketamine (ip, 100 mg/kg, Fujian Gutian Pharmaceutical Co., Ltd.) and xylazine (8 mg/kg, Sigma). Subsequently, they were fixed and then left ventricular end diastolic diameter (LVEDD), left ventricular end systolic diameter (LVESD), left ventricular ejection fraction (LVEF), and left ventricular fractional shortening (LVFS) were measured using an echocardiography system [42].

Next, blood was collected through cardiac puncture and serum was prepared. Then, LDH and creatine kinase (CK)-MB activities, and iron contents in the serum were determined. Mice were euthanized and the hearts were rapidly harvested. The left ventricle was routinely fixed and cut into 5 μ m thickness slices, stained using hematoxylin and eosin (HE), Masson, TUNEL, and dihydroethidium (DHE)/MitoSOX, and observed under a light microscope. The papillary muscle of the left ventricle was fixed and sectioned and observed under a transmission electron microscope (TEM).

The left ventricular lysate was prepared. The contents of iron, MDA, 4-HNE, α -KG, Suc, ATP, GSH and GSSG in the lysate were measured. The expression levels of PTGS2, GPX4, LC3, P62, NDUFB8, and UQCRC2 in the lysate were measured, and the levels of total and phosphorylated AMPK α 2 and ACC in the lysate were evaluated.

2.5. Determination of cell viability

Cell viability was detected with the CCK-8 Cell Counting Kit (TransGen Biotech, FC101) in accordance with the manufacturer's instructions [38].

2.6. Myocardial enzyme determination

LDH activity in the NRCM and H9C2 cell culture medium, and the activities of LDH and CK-MB in the mouse serum were measured using an LDH assay kit (Jiancheng, A020) and CK-MB isoenzyme Assay Kit (Jiancheng, H197) according to the manufacturer's instructions, respectively [15].

2.7. NRCM and H9C2 cell apoptosis and NRCM MMP assessment

NRCM and H9C2 cell apoptosis was assayed with the Annexin V-FITC/PI Apoptosis Detection Kit (BestBio, BB-4101) according to the manufacturer's instructions. Stained cells were analyzed using the

Cytomics FC500 flow cytometer (ex488 nm; em578 nm, Beckman Coulter) [37].

MMP was detected with JC-1 (BestBio, BB-4105) according to the manufacturer's instructions. Stained NRCMs were measured with the flow cytometer (Beckman Coulter) at 530/580 nm (red) and 485/530 nm (green). The ratio of red/green fluorescence intensity represents the MMP level of NRCMs [37,38].

2.8. Iron content detection

To detect the iron contents of the NRCM and H9C2 cell lysates (in vitro) or the lysates of the mouse myocardium and serum (in vivo), the Iron Assay Kit (ab83366; Abcam) was used in accordance with the manufacturer's instructions [43].

2.9. Caspase-3 activity assay

In the myocardial lysate (in vivo) or NRCMs and H9C2 cells (in vitro), caspase-3 activity was assayed with the Caspase-3 Assay Kit (ab39401; Abcam) in accordance with the manufacturer's instructions [15].

2.10. Lipid peroxidation assay

The contents of the lipid peroxidation products MDA and 4-HNE in H9C2 lysates were assessed with the Lipid Peroxidation (MDA) Assay Kit (MAK085, Sigma) and the Lipid Peroxidation (4-HNE) Assay Kit (ab238538, Abcam) in accordance with the manufacturer's instructions, respectively [44].

2.11. Evaluation of the activities of complexes I and III in the mitochondrial ETC and tricarboxylic acid (TCA) cycle

Mitochondria were isolated from NRCMs using the Mitochondria Isolation Kit for Cultured Cells (ab110170, Abcam). The activities of complexes I and III in the mitochondrial ETC were assessed with the Complex I Enzyme Activity Assay Kit (ab109721, Abcam) and the Mitochondrial Complex III Activity Assay Kit (K520-100, Biovision) according to the manufacturer's instructions, respectively [44].

The contents of α -KG and Suc were measured using the α -Ketoglutarate Assay Kit (MAK054, Sigma) and the Succinate Colorimetric Assay Kit (MAK184, Sigma) in accordance with the manufacturer's instructions, respectively [44].

2.12. MDC and LysoTracker red staining

NRCMs were plated in 24-well plates (1×10^4 cells/cover slip) and treated with the abovementioned method, and incubated using the fluorescence dye Dansylcadaverine (MDC, 30432, Sigma) or LysoTracker Red DND-99 (L7528, Invitrogen) in accordance with the manufacturer's instructions, respectively. Subsequently, fluorescence microscopy (Olympus) was used to observe the related changes [38].

2.13. Measurement of the GSH and GSSG contents

The contents of the nonenzymatic antioxidant system (GSH, GSSG, and GSH/GSSG ratio) were evaluated using the GSH and GSSG Assay Kit (S0053, Beyotime) in accordance with the manufacturer's instructions [38].

2.14. Measurements of intracellular/mitochondrial ROS

H9C2 cells were plated in 24-well plates (1×10^4 cells/cover slip) and treated with the abovementioned method, and incubated using DHE (47051, BestBio) or MitoSOX (M36008, Invitrogen) according to the manufacturer's instructions respectively. Next, fluorescence microscopy

(Olympus) was used to observe the related changes [38].

2.15. Measurement of OCR and ECAR

NRCMs were seeded in Seahorse XFp cell cultured miniplates (Agilent, 103725-100, 5×10^4 cells/well) and treated with the abovementioned method. OCR and ECAR were assayed using the Mito Stress Test Kit (Agilent, 103015-100) and the Glycolysis Stress Test Kit (Agilent, 103020-100) by the XFp Extracellular Flux Analyzer (Agilent), as previously described [37].

2.16. Echocardiography

Before measuring, mice were anesthetized and fixed. The M curves were measured at the papillary muscle long axis and left ventricle section level using an echocardiography system (V6, 23 MHz linear transducer, VINNO) for three consecutive cardiac cycles. LVESD, LVEDD, LVSV, and LVDV were measured. LVEF and LVFS were calculated as follows: LVEF = (LVDV - LVSV)/LVDV \times 100%; LVFS = (LVDD - LVSD)/LVDD \times 100%. Three measurements were made and then the mean value was calculated [42].

2.17. Morphology examination

The left ventricle was placed in a 10% formaldehyde solution and then cut into 5 μ m thick sections. HE (Sigma, MHS1), Masson (Sigma, 1.00485) and TUNEL (Promega, G7360) staining was performed as previously described [15,19]. Next, the slices were observed using a microscope (Olympus).

2.18. Measurement of ATP production

A total of 10 mg myocardium was homogenized in 100 μ l of ATP assay buffer, centrifuged, and then the supernatant was deproteinated. The ATP contents of samples were measured with the ATP Assay Kit (Abcam, ab83355) according to the manufacturer's instructions [45].

2.19. Ultrastructural assessment

At the end of the in vitro experiments, NRCMs were collected, prefixed with 2.5% glutaraldehyde overnight, and postfixed with 2% osmium tetroxide, then dehydrated, embedded, ultrathin sectioned, stained, and observed with TEM (H-1650, HITACHI).

At the end of the in vivo experiments, the fresh left ventricle papillary muscle sample (1 mm³) was immediately collected and fixed for 4 h. Then, the sample was permeated, dehydrated, embedded, ultrathin sectioned, and observed with TEM (HITACHI).

The mitochondrial ultrastructural damage was assessed based on the Fameng method [46].

2.20. Western blot analysis

At the determined time, proteins from the lysates of the myocardium (in vivo) and NRCMs and H9C2 cells (in vitro) were extracted using the Total Protein Extraction Kit (Applygen, P1250) and quantified using the BCA Assay Kit (Thermo, 23225). Protein expression was analyzed as previously described [37,38]. Briefly, 30 μ g protein was separated by SDS-PAGE (Sigma, PCG2001) and transferred onto polyvinylidene fluoride membranes (Bio-Rad, 1704273). The membranes were blocked with 5% bull serum albumin, and subsequently overnight at 4 $^{\circ}$ C with the primary antibodies: PTGS2 (1:500), GPX4 (1:1000), LC3 (1:1000), P62 (1:500), AMPK α 2 (1:1000), p-AMPK α 2 (1:1000), mTOR (1:1000), p-mTOR (1:1000), ULK1 (1:1000), p-ULK1 (1:1000), ACC (1:500), p-ACC (1:500), NDUFB8 (1:500), UQCRC2 (1:500), β -actin (1:1000), and GAPDH (1:1000). Subsequently, the membranes were incubated with horseradish peroxidase-conjugated secondary antibodies (1:2000).

GAPDH and β -actin were the internal controls. Finally, protein bands were imaged and analyzed with the Quantity One software (Bio-Rad) [38].

2.21. Statistical analysis

Data are shown as the mean \pm standard deviation (SD) and analyzed using the SPSS20.0 software (IBM). One-way analysis of variance followed post-hoc Tukey's honestly significant difference test was used to compare the groups. $p < 0.05$ was considered statistically significant.

3. Results

3.1. EGCG pretreatment alleviates cardiomyocyte ferroptosis associated with DIC

Recent studies have shown that ferroptosis is the primary form of RCD in DIC [8,23]. We have reported that some phytochemicals, such as curcumin [15], quercetin [14], tetramethylpyrazine [13], and kaempferol [12], alleviate the cell damage caused by DIC and Dox-induced endotheliotoxicity [11]. To confirm whether EGCG treatment alleviates ferroptosis and protects cardiomyocytes against DIC, we used NRCMs and H9C2 cells, a cardiomyocyte-like cell line, to establish models of the cell damage caused by DIC. Firstly, the time-effect relationship of EGCG protection was explored (Fig. S1). Results showed that the strongest protection was achieved with EGCG pretreatment for 36 h, which offered a level of protection similar to that of 24 h pretreatment. The protection following EGCG pretreatment for 12 h was weaker, whereas EGCG synchronous co-treatment protection continued to weaken. The protective effect of EGCG post-treatment for 12 h was the weakest (Fig. S2). Therefore, EGCG pretreatment for 24 h was selected for the subsequent experiments. Our results further revealed that after pretreatment with different concentrations of EGCG (5, 10, 20, 40, or 80 μ M) for 24 h, NRCM and H9C2 cell viability/LDH activity were higher/lower than those of cells subjected to Dox toxicity in a concentration-dependent manner (Fig. S3). We selected 20 μ M EGCG as the pretreatment concentration in the subsequent experiments (Fig. 1C).

As shown in Fig. 1D and E, in NRCMs and H9C2 cells pretreated with 20 μ M EGCG, apoptosis and caspase-3 activity were significantly decreased, suggesting that 20 μ M EGCG pretreatment could protect NRCMs and H9C2 cells against DIC. Interestingly, similar results were obtained using 2 μ M of the ferroptosis inhibitor Fer-1 [47] and 100 μ M of the iron chelator Dxx [48] in NRCMs and H9C2 cells co-treated with 1 μ M Dox (Fig. 1C–E), suggesting that the protection of EGCG pretreatment was related to alleviating ferroptosis caused by DIC.

Iron dependence is the most important cause and sign of ferroptosis [8–10,22]. Hence, we next measured the iron content of NRCM and H9C2 cell lysates. The iron content of the Dox-treated group was significantly increased. The iron content of EGCG-pretreated cells was similar to that of Fer-1 and Dxx co-treated cells, in which the increase of iron content caused by 1 μ M Dox exposure was neutralized (Fig. 1F).

To further verify that EGCG pretreatment alleviated the ferroptosis caused by DIC in NRCMs and H9C2 cells, we evaluated PTGS2 (a positive molecular marker of ferroptosis) [19] and GPX4 (a negative molecular marker of ferroptosis) [9] in the cell lysates of the different treatment groups. When NRCMs and H9C2 cells were damaged by Dox toxicity, PTGS2 expression was significantly increased, while GPX4 expression was decreased; however, EGCG pretreatment, and Fer-1 and Dxx co-treatment reversed these changes (Fig. 1G and H). TEM observation revealed that the mitochondria in Dox-treated NRCMs were severely distorted, with decreased cristae, that the Fiameng scores, a semiquantitative evaluation method of the mitochondrial ultrastructure [46], significantly increased, and that these Dox-induced effects were rescued by EGCG pretreatment, and Fer-1 and Dxx co-treatment (Fig. 1I).

These results confirmed that ferroptosis was the main mode of DIC,

and that EGCG pretreatment could effectively alleviate ferroptosis and protect cardiomyocytes.

Interestingly, we further found that EGCG pretreatment could also affect the expression of some autophagy markers [38], namely, upregulate LC3 expression and downregulate P62 significantly in NRCMs and H9C2 cells (Fig. 1J and K), suggesting that the above protective effects of EGCG pretreatment may be related to the activation of autophagy.

3.2. EGCG pretreatment enhances adaptive autophagy in cardiomyocytes injured by Dox toxicity

Some studies have confirmed that autophagy is also one important RCD form involved in DIC [8–10]. Autophagy, ferroptosis, and apoptosis always overlap and crosstalk with each other, determining the final state of cardiomyocytes [8] (Fig. 8A). When we studied the abovementioned time-effect relationship of EGCG protection, we found that the levels of LC3 and P62, two molecular markers of autophagy [38], changed synchronously. Interestingly, the positive changes of LC3 and P62 were the most obvious when EGCG pretreatment for 24 h had the strongest protective effects; in other words, when EGCG activated autophagy most strongly, its protective effects were the most significant (Fig. S2, S4A and S4B).

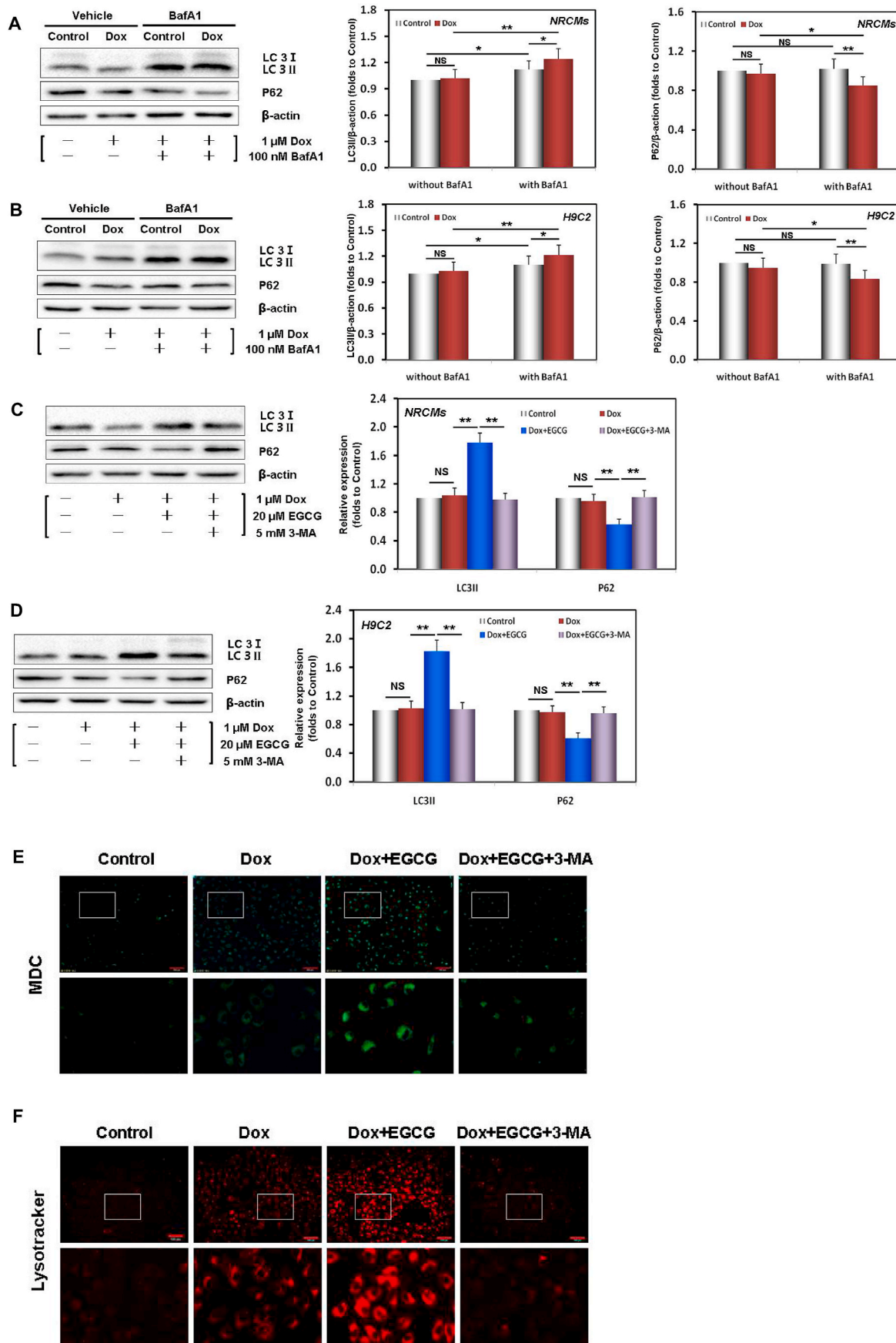
BafA1 can inhibit the fusion between autophagosomes and lysosomes [38]. To identify the effect on LC3 and P62, reflecting the enhancement of autophagy rather than the damage of autophagic flux, NRCMs and H9c2 cells were treated with BafA1. Our results showed that following Dox injury, the expression of LC3/P62 slightly increased/decreased in NRCMs and H9C2 cells (Fig. 2A and B). However, the above differences were increased after co-treatment with BafA1, indicating that Dox injury triggered weak autophagy and did not impair autophagic flux. EGCG pretreatment significantly upregulated LC3 and downregulated P62 expression in NRCMs and H9C2 cells; however, these effects were neutralized by adding 5 mM 3-MA, another autophagy inhibitor (Fig. 2C and D) [39].

MDC (red) and Lyso Tracker Red (green) are markers of early and late autophagy, respectively [38]. In Dox-injured cells, the red/green fluorescent dots were weak, and EGCG pretreatment significantly enhanced the two fluorescence intensities. However, both dots were decreased by adding 3-MA (Fig. 2E). The results not only confirmed the expression of LC3 and P62 (Fig. 2C and D), but also were consistent with the results of cell viability and LDH activity (Figs. S4D and S4E).

Overall, the results suggested that autophagy was involved in DIC and that EGCG pretreatment significantly enhanced autophagy flux and protected cardiomyocytes. The protective effects were reversed by 3-MA.

3.3. EGCG pretreatment upregulates AMPK α 2 and promotes TCA cycle activation in Dox-injured cardiomyocytes

Autophagy usually results from the activation of AMPK and downstream ULK1 and the inhibition of mTOR (a negative regulator of autophagy) pathway [8–10]. To explore whether, during DIC injury, the AMPK α 2-ULK1 and AMPK α 2-mTOR axes participated in the pathophysiological process of activating autophagy and the effects of EGCG pretreatment, we analyzed the expression and phosphorylation of related proteins. As illustrated in Fig. 3A and B, in EGCG-pretreated NRCMs and H9C2 cells, the ratios of *p*-AMPK α 2/AMPK α 2 and *p*-ULK1/ULK1 were higher than those in Dox damaged cells. In contrast, the *p*-mTOR/mTOR ratio was lower than that in Dox damaged cells. However, the phosphorylation of AMPK α 2, ULK1, and mTOR was neutralized by the addition of compound C (an AMPK inhibitor) [38] in NRCMs or by AMPK gene silencing using pAD/AMPK-shRNA [38] in H9C2 cells. This verified that EGCG pretreatment promoted autophagy by upregulating and activating the AMPK α 2-ULK1 axis and inhibiting the mTOR pathway.



(caption on next page)

Fig. 2. EGCG pretreatment enhanced adaptive autophagy in Dox-injured cardiomyocytes. **A** Dox-induced autophagic flux evaluated by the difference in the P62 and LC3 levels between NRCMs subjected or not to treatment with 100 nM BafA1. **B** Dox-induced autophagic flux evaluated by the difference in the P62 and LC3 levels between H9C2 cells subjected or not to treatment with 100 nM BafA1. **C** Western blot bands showing LC3 and P62 protein expression and the relative signal intensities in NRCMs pretreated with 20 μ M EGCG for 24 h and then exposed to 1 μ M Dox, and in cells subjected or not to 20 μ M EGCG and 5 mM 3-MA co-treatment for 48 h; the below findings were also obtained using this method. **D** Western blot bands showing LC3 and P62 protein expression and the relative signal intensities in H9C2 cells. **e** NRCM images stained with MDC. **f** NRCM images stained with LysoTracker Red DND-99. Values are mean \pm SD from three individual experiments. NS, nonsignificant. * $p < 0.05$ compared with the indicated groups. ** $p < 0.01$ compared with the indicated groups. (For interpretation of the references to colour in this figure legend, the reader is referred to the Web version of this article.)

It is noteworthy that with the time-effect changes of the protective effects of EGCG pretreatment alone and the expression of LC3 and P62, *p*-AMPK α 2/AMPK α 2 also showed similar changes (Fig. S2, S4A and S4C). Moreover, with the addition of compound C and *p*AD/AMPK-shRNA, the above changes were basically abolished (Figs. S5A–S5D), but A769962, an AMPK activator [49], had similar protective effects to those of EGCG pretreatment (Figs. S5A and S5B), strongly suggesting that the effects of EGCG pretreatment on enhancing autophagy and protecting cardiomyocytes depended on the upregulation and phosphorylation of AMPK α 2.

Recent studies have revealed that during energy stress, AMPK not only activates autophagy but also improves energy metabolism and promotes fatty acid oxidation [50] and TCA cycle activation [51]. We found that the contents of α -KG and Suc, two key metabolites of the TCA cycle [44], significantly decreased in Dox-injured NRCMs and H9C2 cells, while EGCG pretreatment could effectively reverse these changes (Fig. 3B). In addition, *p*-ACC/ACC, another downstream protein of AMPK α 2 [50], also showed similar changes. Similarly, the effects of EGCG pretreatment were canceled by compound C in NRCMs or by *p*AD/AMPK-shRNA treatment in H9C2 cells, indicating that EGCG pretreatment could improve energy metabolism and promote fatty acid oxidation and the TCA cycle, but that it also depended on AMPK α 2 activity.

3.4. EGCG pretreatment improves redox equilibrium and lipid metabolism in Dox-injured cardiomyocytes

Studies have confirmed that the major source of cell injury that induces DIC, such as ferroptosis, is excess ROS generation in the mitochondria [52]. As illustrated in Fig. 4A, both DHE and MitoSOX fluorescence intensities in H9C2 cells were significantly enhanced as a result of Dox injury, especially that of MitoSOX. EGCG pretreatment, similar to MitoTEMPO treatment, a mitochondrial free radical scavenger [19], weakened both the DHE and MitoSOX fluorescence intensities in H9C2 cells, indicating that EGCG pretreatment inhibited excess ROS generation in Dox-injured H9C2 cells.

Dox-induced injury in cardiomyocytes leads to excess ROS generation, damaging lipids and triggering abnormal lipid metabolism [7,8]. As illustrated in Fig. 4B, following Dox-induced injury, the lipid peroxidation products, namely, both the MDA and 4-HNE contents in H9C2 lysates, were significantly increased. However, EGCG pretreatment, similar to Fer-1, a lipophilic radical trap for ferroptosis [8], and MitoTEMPO pretreatment, could effectively rescue the above changes.

GPX4 is not only a molecular marker of ferroptosis, but also a central link in neutralizing the deleterious effects of ferroptosis-induced lipid peroxidation that uses GSH to clean up excess lipid metabolites. Therefore, GSH deprivation indirectly further inactivates GPX4 [22]. This uncontrolled lipid peroxidation induces and deteriorates cardiomyocyte ferroptosis. Our results revealed that following DIC damage, not only the expression of GPX4 was downregulated in NRCMs and H9C2 cells (Fig. 1G and H), but also GSH was depleted, whereas GSSG significantly increased and the GSH/GSSG ratio decreased in H9C2 cells. EGCG pretreatment, and Fer-1 and MitoTEMPO co-treatment could effectively reverse the above changes (Fig. 4C).

These results confirmed that EGCG pretreatment could effectively improve redox equilibrium and lipid metabolism in DIC. Similarly, these changes were consistent with the changes in cell viability and LDH

activity (Fig. S6).

3.5. EGCG pretreatment maintains and improves mitochondrial function in Dox-injured cardiomyocytes

It is well established that mitochondria are important sites of energy metabolism in cells, and that they may also be one of the downstream target organelles of AMPK [51]. Studies have confirmed that mitochondria are directly involved in Dox cytotoxicity, especially cardiotoxicity, resulting in mitochondrial iron overload and excess ROS generation [52]. As illustrated in Fig. 5A and B, following Dox-induced injury, OCR curve showed a downward trend and ECAR curve presented a reversed trend in NRCMs. This indicated that aerobic metabolism and spare capacity were inhibited, that anaerobic glycolysis and glycolytic capacity were enhanced, and that ATP production decreased and NRCMs were in a state of acidosis. EGCG pretreatment effectively rescued the above Dox-induced damages.

Mitochondrial ETC complexes I and III are essential for maintaining the energy supply of cardiomyocytes, and they are also vulnerable to attack and damage [37]. Our results revealed that not only the expression of NDUFB8 (a subunit of complex I) and UQCRC2 (a subunit of complex III) were downregulated, but also their activities were inhibited in Dox-injured NRCMs compared to those of control cells, and that these Dox-induced effects were rescued by EGCG pretreatment (Fig. 5C and D).

MMP is one of the important indexes to evaluate mitochondrial function. The ratio of red/green fluorescence reflects the voltage difference of MMP [37]. In Dox-injured NRCMs, the red/green ratio reduced to reflect MMP loss, and EGCG pretreatment reversed the loss (Fig. 5E).

These results confirmed that EGCG pretreatment could effectively maintain energy metabolism and improve mitochondrial function in cardiomyocytes injured by DIC. Interestingly, the above protective effects of EGCG pretreatment were canceled by adding compound C, indicating that the effects of EGCG pretreatment depended on AMPK α 2 activity.

It is well known that excess ROS generation and iron- and lipotoxicity-dependency are the three characteristics of ferroptosis [8–10,22]. The above two cardiomyocyte experiments confirmed that EGCG pretreatment could effectively alleviate ferroptosis associated with DIC and protect cardiomyocytes. The underlying mechanism was verified to involve the upregulation and activation of AMPK α 2, which promoted adaptive autophagy, decreased iron accumulation, inhibited oxidative stress and abnormal lipid metabolism, increased the energy supply, and maintained mitochondrial function.

3.6. EGCG pretreatment enhances autophagy and alleviates myocardial ferroptosis in Dox-injured mice

To further confirm the protection of EGCG pretreatment and underlying mechanism in vivo, a DIC model was established in male C57BL/6 mice [15]. Our results showed that in Dox-injured mice, the activities of CK-MB and LDH (two myocardial damage marker enzymes) [15] in serum samples significantly increased, as did the iron content in serum, especially in myocardial tissue (Fig. 6A and C). Echocardiography provided important indices reflecting left ventricular function in mice [42]. The LVEDD and LVESD were enlarged, while the LVEF and

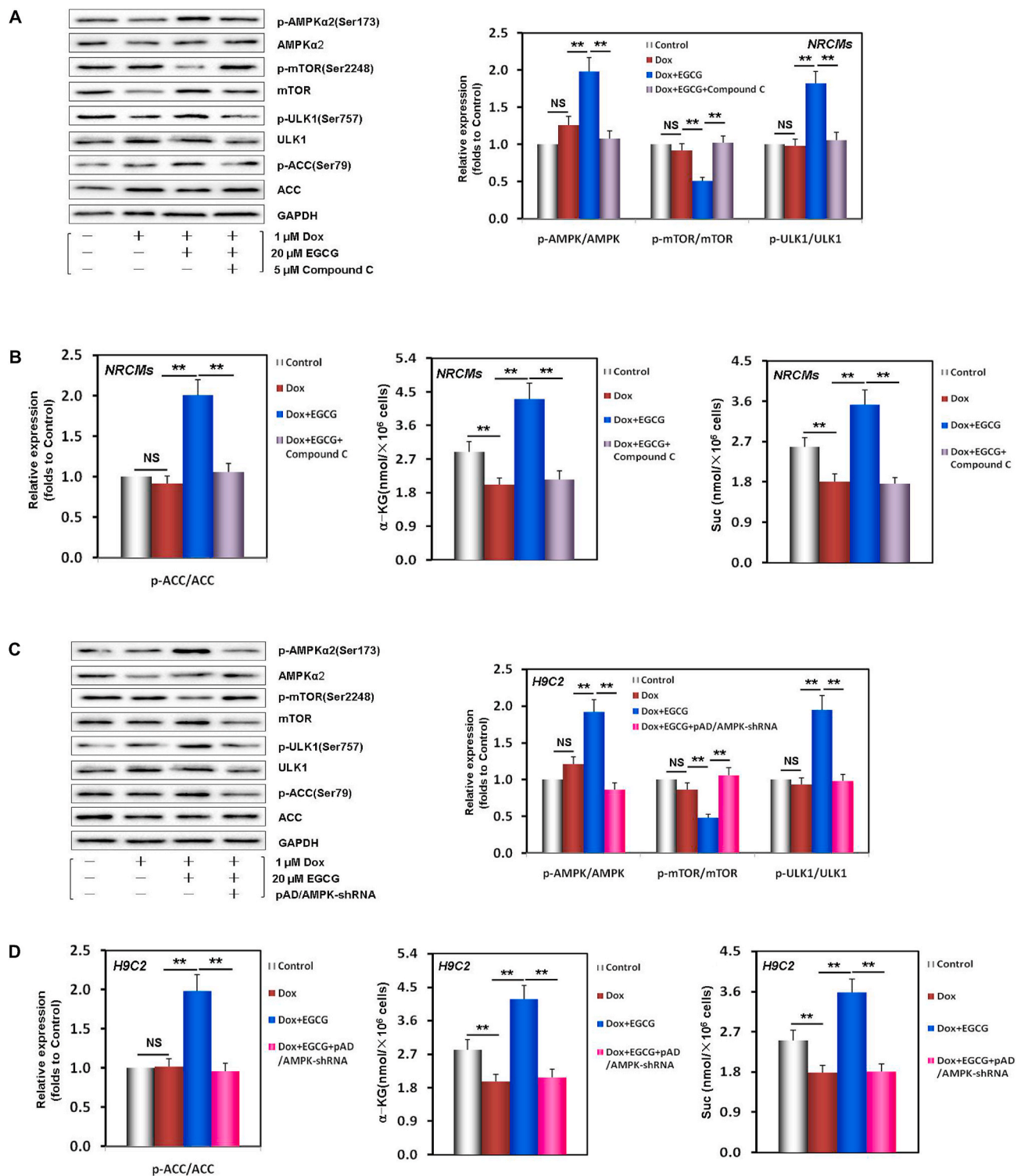


Fig. 3. EGCG pretreatment upregulated AMPK α 2 and promoted TCA cycle activation in Dox-injured cardiomyocytes. **A** Western blot bands showing total and phosphorylated AMPK α 2, mTOR, and ULK1 expression and the relative intensities of *p*-AMPK α 2/AMPK α 2, *p*-mTOR/mTOR, and *p*-ULK1/ULK1 expression in NRCMs pretreated with 20 μ M EGCG for 24 h and then exposed to 1 μ M Dox, and in cells subjected or not to 20 μ M EGCG and 5 μ M compound C co-treatment for 48 h; the below findings were also obtained using this method. **B** The relative intensity of *p*-ACC/ACC and the contents of α -KG and Suc in NRCMs. **C** Western blot bands showing total and phosphorylated AMPK α 2, mTOR, and ULK1 expression and the relative intensities of *p*-AMPK α 2/AMPK α 2, *p*-mTOR/mTOR, and *p*-ULK1/ULK1 expression in H9C2 cells pretreated with 20 μ M EGCG for 24 h and then exposed to 1 μ M Dox, and in cells subjected or not to 20 μ M EGCG and pAD/AMPK-shRNA co-treatment for 48 h; the below findings were also obtained using this method. **D** The relative intensity of *p*-ACC/ACC and the contents of α -KG and Suc in H9C2 cells. Values are mean \pm SD from three individual experiments. NS, nonsignificant. ***p* < 0.01 compared with the indicated groups.

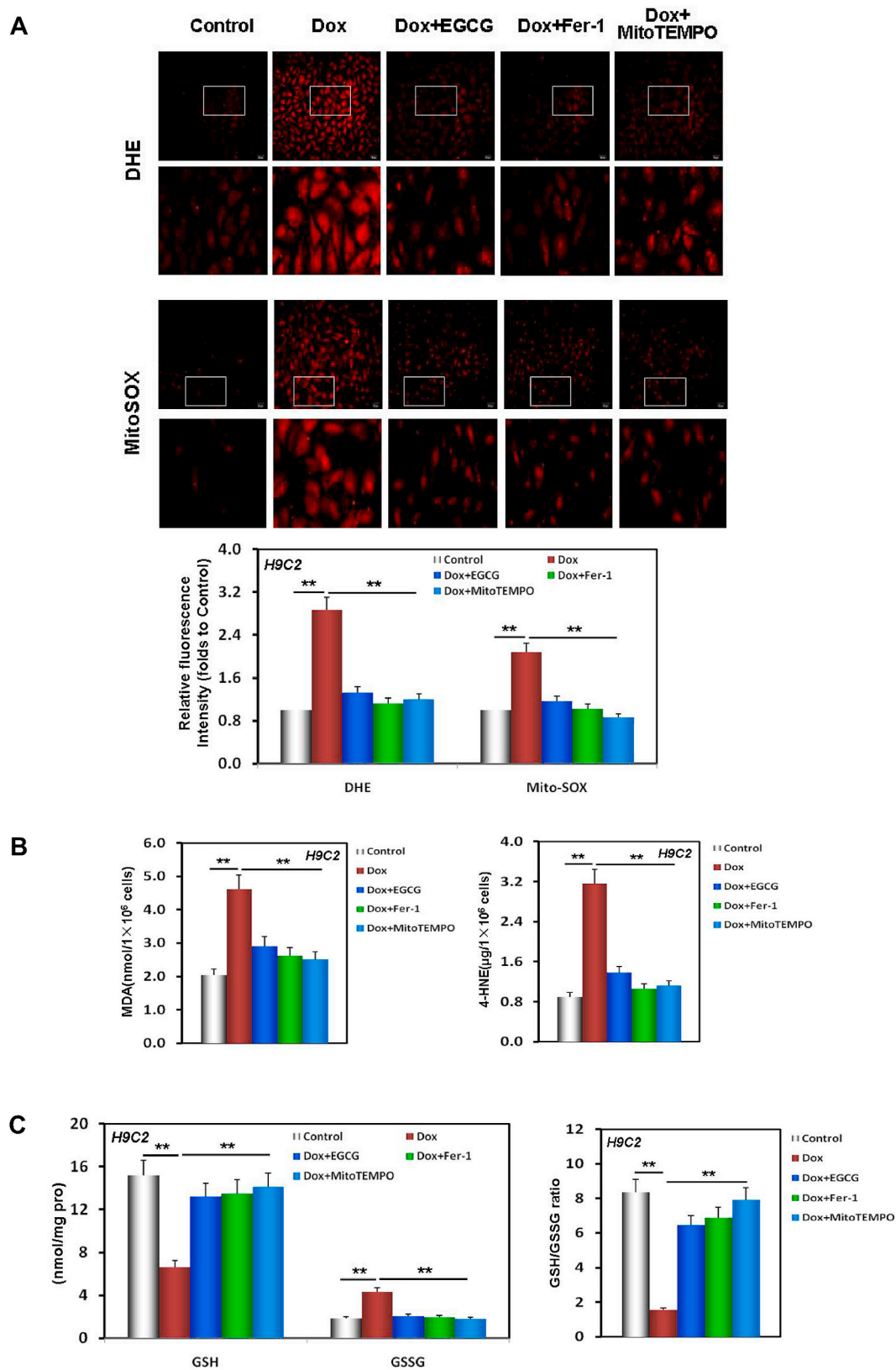


Fig. 4. EGCG pretreatment improved redox equilibrium and lipid metabolism in Dox-injured cardiomyocytes. **A** Images of DHE/MitoSOX probe-stained H9C2 cells and the relative fluorescence intensity of DHE/MitoSOX in H9C2 cells pretreated with 20 μM EGCG for 24 h and then exposed to 1 μM Dox, and in cells subjected or not to 20 μM EGCG, 2 μM Fer-1, and 10 μM MitoTEMPO co-treatment for 48 h; the below findings were also obtained using this method. **B** The MDA and 4-HNE contents in H9C2 cells. **C** The levels of GSH, GSSG, and the GSH/GSSG ratio in H9C2 cells. Values are mean \pm SD from three individual experiments. $**p < 0.01$ compared with the indicated groups.

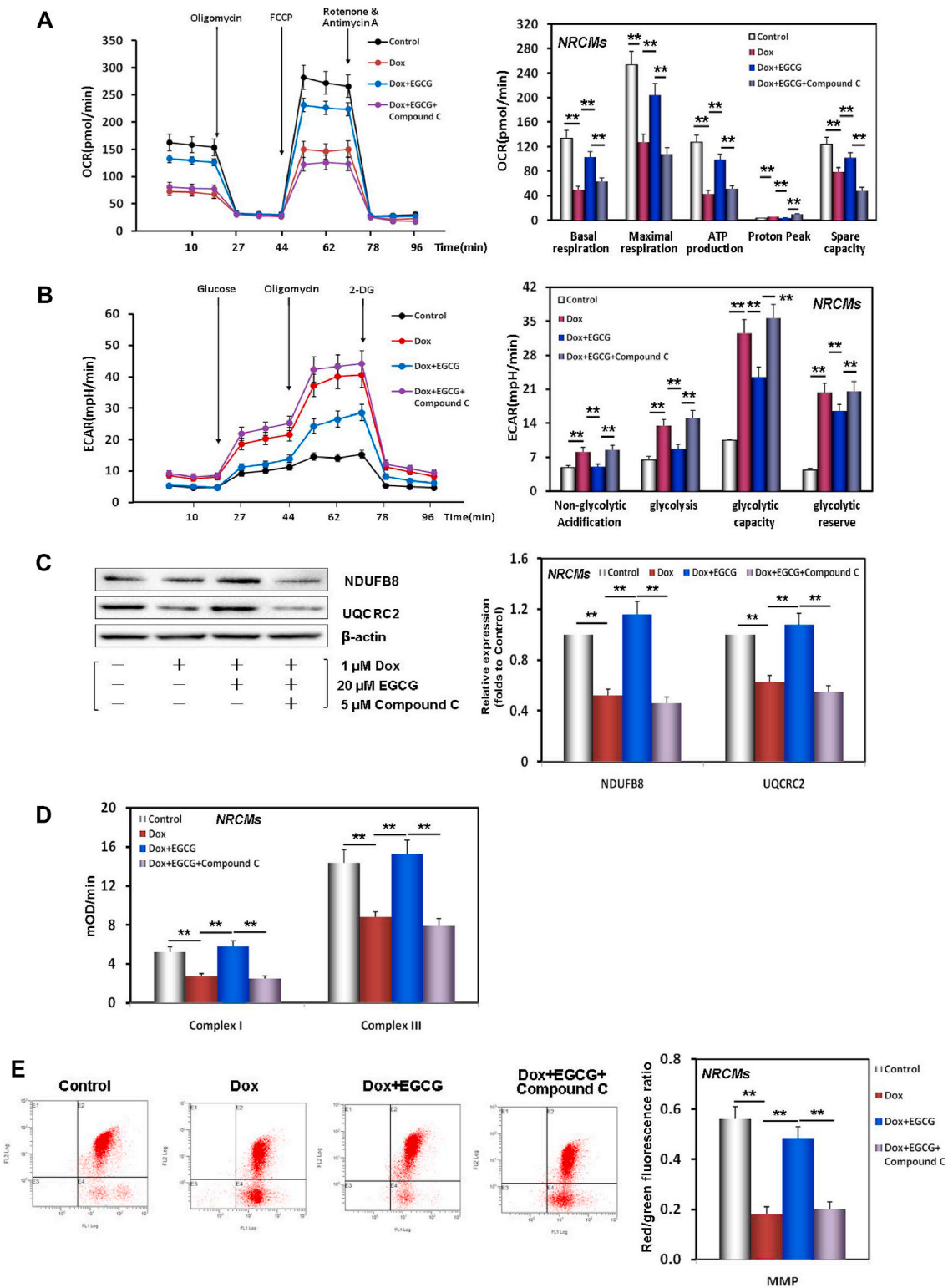


Fig. 5. EGCG pretreatment maintained and improved mitochondrial function in Dox-injured cardiomyocytes. **A** OCR curve charts and the histogram of indices related to mitochondrial vitality in NRCMs pretreated with 20 μ M EGCG for 24 h and then exposed to 1 μ M Dox, and in cells subjected or not to 20 μ M EGCG and 5 μ M compound C co-treatment for 48 h; the below findings were also obtained using this method. **B** ECAR curve charts and the histogram of indices related to mitochondrial glycolytic function in NRCMs. **C** Western blot bands showing NDUFB8 and UQCRC2 protein expression and the relative signal intensities in NRCMs. **D** The activities of complexes I and III in the ETC of mitochondria in NRCMs. **E** MMP levels detected by JC-1 in NRCMs indicated by the red/green fluorescence ratio. Values are mean \pm SD from three individual experiments. $**p < 0.01$ compared with the indicated groups. (For interpretation of the references to colour in this figure legend, the reader is referred to the Web version of this article.)

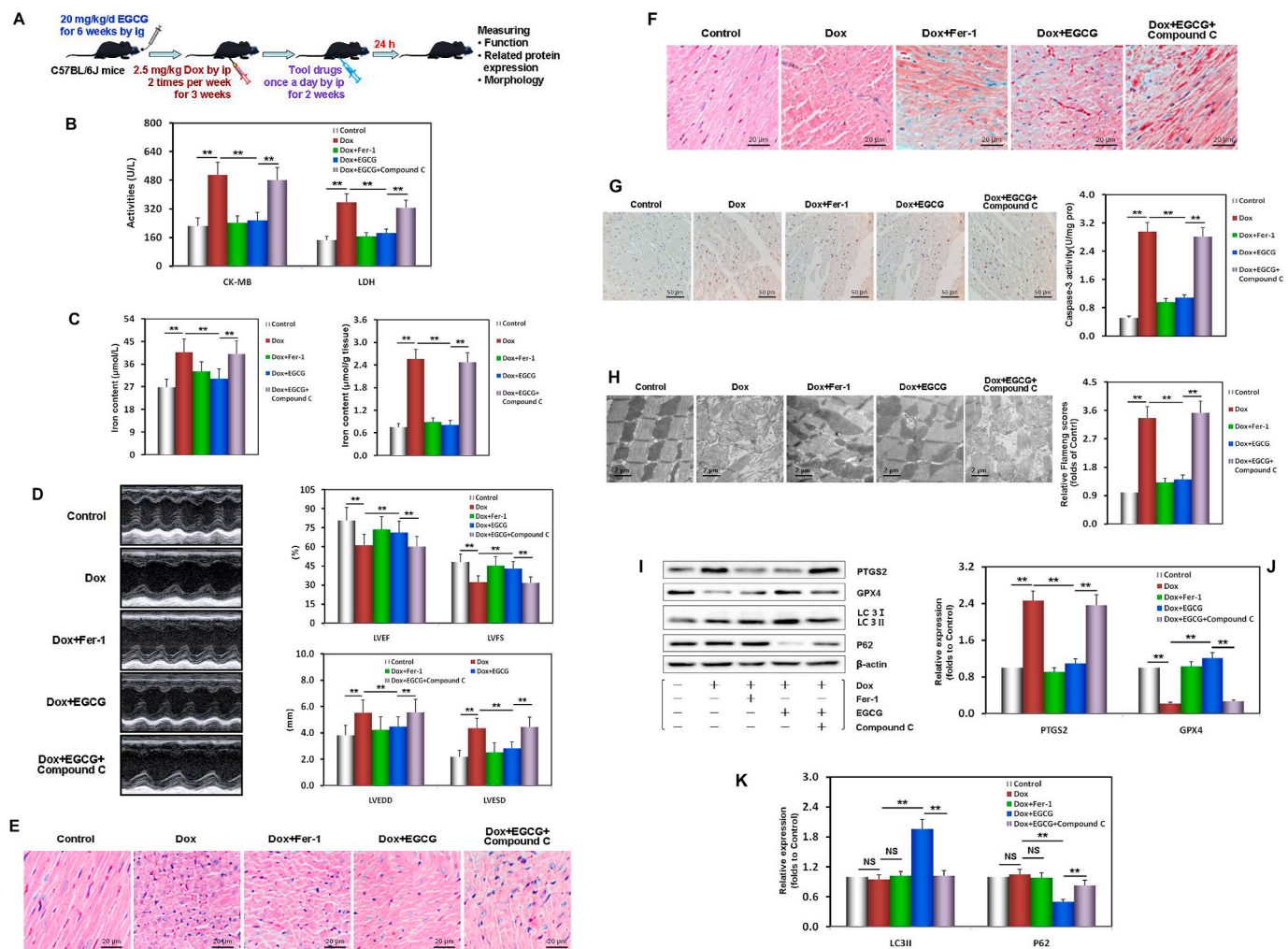


Fig. 6. EGCG pretreatment enhanced adaptive autophagy and alleviated Dox-induced myocardial ferroptosis in mice. **A** Diagram of the in vivo study design. **B** CK-MB and LDH activity in mouse serum in each treatment group. **C** The iron contents of mouse serum and myocardium in each treatment group. **D** Echocardiographic images, and the histogram of LVEDD, LVESD, LVEF, and LVFS parameters in mice. Values are mean \pm SD from six individual experiments. $**p < 0.01$ compared with the indicated groups. **E** Images of HE-stained mouse myocardium. **F** Images of Masson-stained mouse myocardium. **G** Images of TUNEL-stained mouse myocardium. **H** Transmission electron microscope images and the relative Fiameng scores of mouse myocardium. **I** Western blot bands showing PTGS2, GPX4, LC3, and P62 protein expression in mouse myocardium. **J** Relative intensities of PTGS2 and GPX4 expression in mouse myocardium. **K** Relative intensities of LC3 and P62 expression in mouse myocardium. Values are mean \pm SD from three individual experiments. NS, nonsignificant. $**p < 0.01$ compared with the indicated groups.

LVFS were inversely diminished, indicating that the cardiac function of mice was seriously damaged (Fig. 6D). As expected, EGCG pretreatment, similar to Fer-1 pretreatment, neutralized these abnormal functional and enzymatic indices in mice with DIC-induced damage (Fig. 6B–D).

Further morphological evaluation and analysis showed that following the Dox-induced injury, the myocardial tissues of the mice showed inflammatory infiltration, cellular swelling, and interstitial cell hypertrophy, as demonstrated with HE staining (Fig. 6E), a disordered arrangement of myocardial fibers and large amounts of collagen deposition, as demonstrated with Masson staining (Fig. 6F), and many noticeable brown TUNEL-positive cardiomyocytes, as demonstrated with TUNEL staining. Meanwhile, the myocardial lysate caspase-3 activity significantly increased (Fig. 6G), mitochondria became severely distorted, mitochondrial cristae decreased, and Fiameng scores significantly increased (Fig. 6H), indicating that the cardiac structure of mice was seriously damaged. Similarly, EGCG pretreatment, similar to Fer-1 pretreatment, could effectively rescue and alleviate the above morphological myocardial changes in mice with cardiac damage caused by DIC (Fig. 6E–H).

Subsequently, Western blot analysis revealed that two molecular markers of ferroptosis, PTGS2 and GPX4, showed a similar change trend

as that observed in vitro (Fig. 6I and J); that is, PTGS2 and GPX4 expression was significantly upregulated/downregulated in the DIC mouse myocardium, and EGCG and fer-1 pretreatment could basically neutralize the above changes. However, two autophagy molecular markers, LC3 and P62, showed no significant difference in the myocardium of mice exposed to Dox toxicity. EGCG pretreatment upregulated LC3 expression and downregulated P62 expression, but Fer-1 had no effect on either of them (Fig. 6I and K). The above results indicated that in vivo EGCG pretreatment alleviated ferroptosis caused by DIC, and that this involved the activation of myocardial adaptive autophagy.

Importantly, all the above protective effects of EGCG pretreatment could be abolished by compound C, suggesting that they depended on AMPK α 2 activity.

3.7. EGCG pretreatment upregulates AMPK α 2 and improves redox equilibrium and mitochondrial function in the myocardium of mice injured by Dox-induced toxicity

To further verify the mechanism of EGCG pretreatment against DIC in vivo, EGCG pretreatment effects on AMPK α 2 expression and

phosphorylation, energy metabolism, oxidative stress and lipid metabolism, and mitochondrial function in the mouse myocardium after 6 weeks were evaluated. We found that *p*-AMPK α 2/AMPK α 2 and *p*-ACC/ACC ratios significantly increased with EGCG pretreatment, but with Fer-1, both of them increased slightly (Fig. 7A), while the levels of two key metabolites of the TCA cycle, α -KG and Suc, significantly increased with EGCG pretreatment or Fer-1 co-treatment (Fig. 7B). The expression levels of NDUFB8 and UQCRC2, and the production of ATP also significantly increased with EGCG pretreatment or Fer-1 co-treatment (Fig. 7A, C and 7D). These results suggested that EGCG pretreatment improved myocardial energy metabolism by upregulating and activating AMPK α 2 and promoting the TCA cycle. However, Fer-1 was responsible for the maintenance of mitochondrial function.

The following indices: DHE/MitoSox staining, GSH and GSSG contents, GSH/GSSG ratio, MDA and 4-HNE contents, reflecting redox equilibrium and lipid metabolism of myocardial tissue and its mitochondria, were mostly consistent with those in the in vitro results (Fig. 7E–I). Similarly, the above protective effect of EGCG pretreatment was nullified by adding compound C, indicating that the effects of EGCG pretreatment depended on AMPK α 2 activity (Fig. 7A–I).

4. Discussion

With the increasing number of malignant tumor survivors, the multiple chemotherapy-related cytotoxicities, especially cardiotoxicity, represent an increasingly serious health problem [1,2]. It has been confirmed that the mechanism of DIC is very complex, involving a variety of RCD forms, including necroptosis, pyroptosis, autophagy, ferroptosis, and apoptosis, and that these forms not only occur simultaneously, but also overlap and crosstalk with each other [8–10] (Fig. 8A). Clarifying the relevant mechanisms is essential for exploring effective therapies and identifying pharmacological agents [7]. Furthermore, the failure of laborious clinical trials of some agents that were expected to inhibit excess ROS generation confirms the complexity of the underlying mechanisms and necessity to elucidate them [1,6,10,53,54]. In this study, we found in vitro and in vivo that at least autophagy, apoptosis, and ferroptosis were involved in DIC according to

multiple functional, enzymatic, and morphological indices.

Complexity creates difficulties, but it can also bring opportunities. Studies have shown that some small molecule agents have multiple targets, which can simultaneously interfere with multiple pathways and induce pharmacological effects [7,10]. For example, berberine could protect cardiomyocytes against DIC by regulating autophagy and inhibiting apoptosis [55–57]. Dxz is the only drug approved by FDA for clinical use in the treatment of DIC [52]. It is generally believed that Dxz, as an iron chelator, can reduce the iron content of cardiomyocytes associated with Dox-induced toxicity [58]. However, studies have found that Dxz could also prevent DNA damage caused by Dox-induced toxicity via depleting topoisomerase II β [59]. Therefore, it is expected to find multi-target agents that can interfere with the multiple forms of RCD related to Dox cardiotoxicity [7,10]. We believe that EGCG is a candidate phytochemical. A large number of studies have demonstrated that EGCG could affect the expression of specific proteins and signal pathways, such as AMPK and related pathways [28,30,60–62], and intervene in a variety of RCD forms, such as autophagy, apoptosis, and ferroptosis [34–36,63–65], all of which confirm its pharmacological characteristics, multiple targets, and underlying mechanisms [24,25]. Our results revealed that in DIC, EGCG pretreatment effectively decreased iron accumulation, inhibited excess ROS generation and oxidative stress, and rectified abnormal lipid metabolism in vitro and in vivo, which was similar to the intervention effects of the ferroptosis inhibitor Fer-1 [19,20], iron chelator Dxz [52,58], and mitochondrial free radical scavenger MitoTEMPO [18,19]. According to the three biological characteristics of ferroptosis [8–10,22], we confirmed that EGCG pretreatment could alleviate ferroptosis and protect the myocardium against Dox-induced toxicity.

Autophagy is a homeostatic process of degradation and recycling of cellular components, usually considered as a pro-survival mechanism under normal conditions or under a variety of cellular stresses [8–10,66,67]. Many studies on the role of autophagy in DIC have reported conflicting findings. Whereas some have reported protective effects, others have shown that blocking autophagy leads to alleviation of DIC. This difference may primarily depend on the phase of autophagy; Dox dosage and duration; the dosage, phase, and duration of intervention factors;

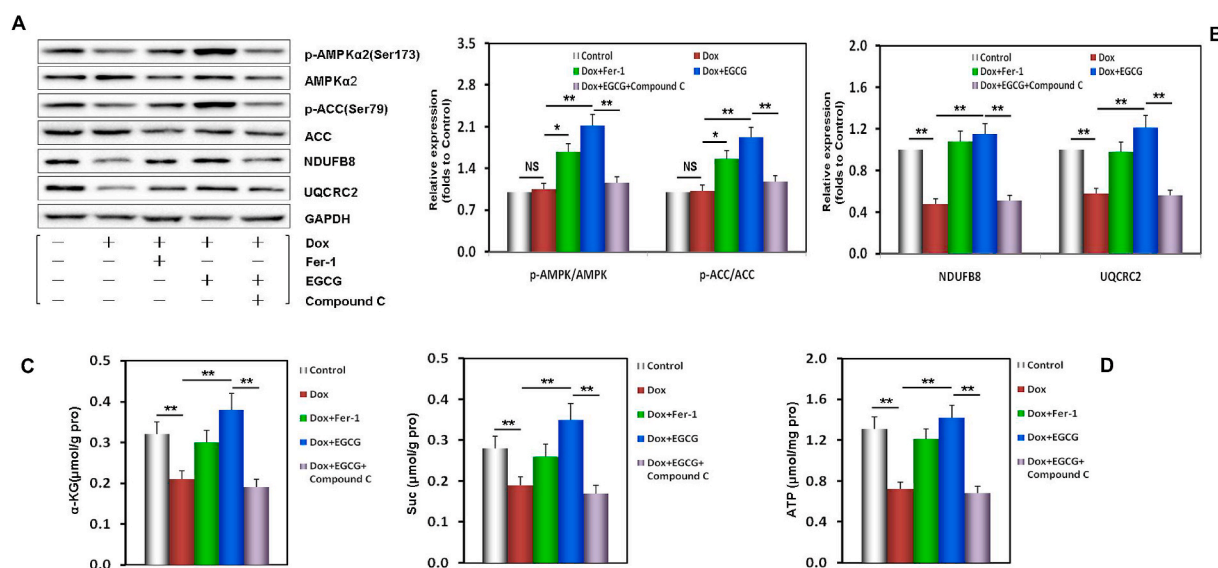


Fig. 7. EGCG pretreatment upregulated AMPK α 2 and improved redox equilibrium and mitochondrial function in the Dox-injured mouse myocardium. **A** Western blot bands showing total and phosphorylated AMPK α 2 and ACC expression, NDUFB8 and UQCRC2 expression, and the relative intensities of *p*-AMPK α 2/AMPK α 2 and *p*-ACC/ACC expression in the mouse myocardium. **B** Relative intensities of NDUFB8 and UQCRC2 expression in the mouse myocardium. **C** The contents of α -KG and Suc in the mouse myocardium. **D** The ATP contents in the mouse myocardium. **E** DHE/MitoSOX probe-stained images and the relative fluorescence intensity of DHE/MitoSOX in the mouse myocardium. **F** The levels of GSH, GSSG, and the GSH/GSSG ratio in the mouse myocardium. **G** The MDA contents in the mouse myocardium. **H** The 4-HNE contents in the mouse myocardium. Values are mean \pm SD from three individual experiments. NS, nonsignificant. * p < 0.05 compared with the indicated groups. ** p < 0.01 compared with the indicated groups.

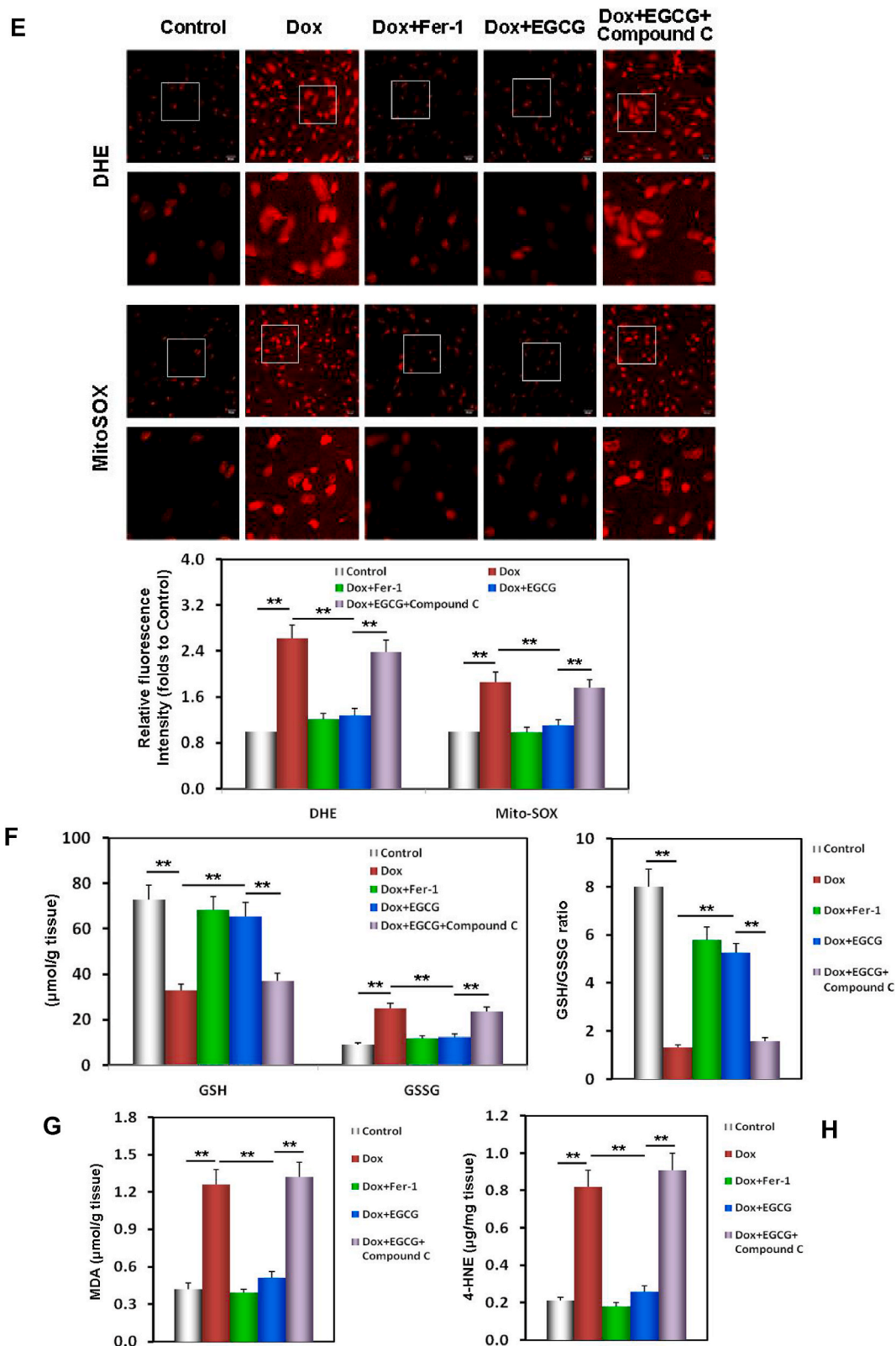


Fig. 7. (continued).

and other factors [7,10]. Studies have confirmed that autophagy can be divided into autophagy-dependent cell death and adaptative autophagy [8–10]. Recent evidence has verified that induction of autophagy (adaptative autophagy) prior to Dox treatment could make cells more tolerant to Dox toxicity by removing damaged cell components. For

instance, before Dox exposure, stimulation of autophagy by caloric restriction or inhibition of mTOR activity could improve cardiac outcome and reduce mortality in model animals [68–72]. We found that EGCG pretreatment for 24 h, that is, 24 h before Dox stimulation, showed the best protective effects. With the shortening of pretreatment time, the

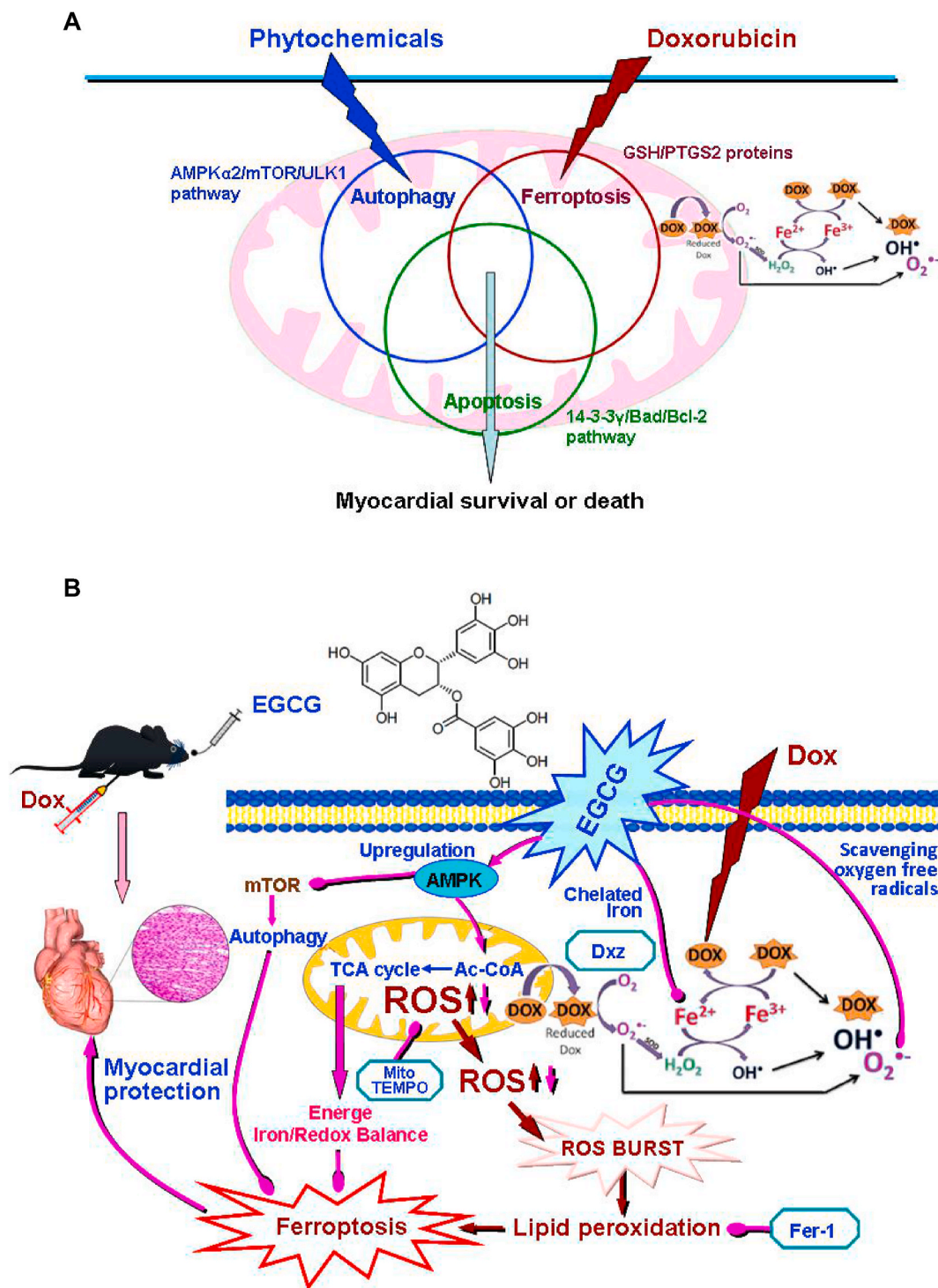


Fig. 8. Schematic diagram of related hypothesis. A. Schematic diagram of “Autophagy, iron ptosis and apoptosis always overlap and interfere with each other” and the protein and signal pathway hypothesis related to the study. B. Schematic diagram showing how EGCG pretreatment protected cardiomyocytes against Dox-induced ferroptosis. EGCG pretreatment upregulated the expression and phosphorylation of AMPK α 2 and activated adaptive autophagy, thereby decreasing iron accumulation, inhibiting excess ROS generation and abnormal lipid metabolism, increasing energy supply, and maintaining mitochondrial function, ultimately protecting the myocardium against Dox-induced ferroptosis.

protective effects significantly decreased. Interestingly, LC3 and P62, two autophagy markers [10,38], showed synchronous positive changes; that is, the duration of EGCG pretreatment was positively correlated with its protective effects and activation of autophagy. It should be noted that the protective effects of EGCG pretreatment were almost cancelled by adding the autophagy inhibitor 3-MA [38,39], which confirmed that these protective effects depended on adaptive

autophagy activation in cardiomyocytes before Dox stimulation.

Studies have confirmed that Dox is transformed into highly oxidative metabolites in mitochondria and induces redox imbalance [52]. There are many reports that mitochondrial mediated DIC causes apoptosis, and mitochondria have also become crucial targets for possible intervention [73–76]. Our previous studies have found that some phytochemicals upregulated 14-3-3 γ expression, phosphorylated

Bad, promoted the migration of Bcl-2 to mitochondria, reduced mPTP openness, inhibited apoptosis of cardiomyocytes and vascular endothelial cells, and resisted Dox toxic injury [12–15]. This study revealed that EGCG pretreatment activated adaptive autophagy, improved redox equilibrium, maintained MMP, and alleviated apoptosis by DIC induced.

At present, it is believed that adaptive autophagy usually originates from AMPK phosphorylation, leading to the formation of complexes by phosphorylated ULK1 and inhibiting mTOR phosphorylation, and that the two act together to activate adaptive autophagy [8–10,23]. Our results revealed that EGCG pretreatment significantly activated the AMPK α 2-ULK1 axis and inhibited the AMPK α 2-mTOR axis, thereby activating adaptive autophagy and protecting cardiomyocytes against DIC. Notably, the protective effect of EGCG pretreatment was nullified by compound C or pAD/AMPK-shRNA treatment; however, A76962 (AMPK activator) treatment [49] showed similar protective effects to those of EGCG pretreatment. Therefore, we emphasized that the effects of EGCG pretreatment on enhancing autophagy and protecting cardiomyocytes depended on the upregulation and phosphorylation of AMPK α 2.

The latest studies have found that AMPK not only activates autophagy during energy stress, but also improves energy metabolism and promotes fatty acid oxidation and the TCA cycle [50,51]. In this study, we demonstrated that EGCG pretreatment upregulated and phosphorylated ACC, another downstream protein of AMPK α 2, promoted the TCA cycle and increased energy supply. Hence, cardiomyocytes had sufficient energy supply, and redox equilibrium, lipid metabolism, and mitochondrial function could be improved and maintained, and the ability to resist Dox damage was enhanced.

5. Conclusion

In summary, EGCG pretreatment upregulated the expression and phosphorylation of AMPK α 2 and activated adaptive autophagy, thus decreasing iron accumulation, inhibiting excess ROS generation and abnormal lipid metabolism, increasing energy supply, and maintaining mitochondrial function, ultimately protecting the myocardium against DIC-induced ferroptosis (Fig. 8).

Declaration of competing interest

The authors declare that they have no conflict of interest.

Acknowledgements

We would like to thank Editage (www.editage.cn) for English language editing.

Appendix A. Supplementary data

Supplementary data to this article can be found online at <https://doi.org/10.1016/j.redox.2021.102185>.

Author contributions

Study design: MH, HH and DY; experiment conduct: HH, LW, YQ, BY and DY; material preparation: LW, YQ and BY; data collection and analysis: HH, LW, YQ and BY; drafting manuscript: HH and DY; revising manuscript content: MH; supervised the study: MH.

Funding

This work was supported by the Natural Science Foundation of China (82160685 and 81803534 to Huan He, 81673431 to Ming He).

Ethics approval

All animal procedures abided by the National Institutes of Health (USA) guidelines and were authorized by the ethics committee of Nanchang University (No. 2020-0182).

Consent to participate/Consent for publication

The manuscript does not contain clinical studies or patient data.

Availability of data and materials

All data needed to evaluate the conclusions in the paper are present in the paper and/or the Supplementary Materials. Additional data related to this paper may be requested from the authors.

References

- [1] K.D. Miller, L. Nogueira, A.B. Mariotto, J.H. Rowland, K.R. Yabroff, C.M. Alfano, et al., Cancer treatment and survivorship statistics, *CA A Cancer J. Clin.* 69 (2019) 363–385, <https://doi.org/10.3322/caac.21565>, 2019.
- [2] Global Burden of Disease Cancer Collaboration, C. Fitzmaurice, D. Dicker, A. Pain, H. Hamavid, M. Moradi-Lakeh, et al., The global Burden of cancer 2013, *JAMA Oncol.* 1 (2015) 505–527, <https://doi.org/10.1001/jamaoncol.2015.0735>.
- [3] M. Volkova, R. 3rd Russell, Anthracycline cardiotoxicity: prevalence, pathogenesis and treatment, *Curr. Cardiol. Rev.* 7 (2011) 214–220, <https://doi.org/10.2174/157340311799960645>.
- [4] S.M. Swain, F.S. Whaley, M.S. Ewer, Congestive heart failure in patients treated with doxorubicin: a retrospective analysis of three trials, *Cancer* 97 (2003) 2869–2879, <https://doi.org/10.1002/cncr.11407>.
- [5] S. Zhang, X. Liu, T. Bawa-Khalife, L.S. Lu, Y.L. Lyu, L.F. Liu, et al., Identification of the molecular basis of doxorubicin-induced cardiotoxicity, *Nat. Med.* 18 (2012) 1639–1642, <https://doi.org/10.1038/nm.2919>.
- [6] L. Gianni, E.H. Herman, S.E. Lipshultz, G. Minotti, N. Sarvazyan, D.B. Sawyer, Anthracycline cardiotoxicity: from bench to bedside, *J. Clin. Oncol.* 26 (2008) 3777–3784, <https://doi.org/10.1200/JCO.2007.14.9401>.
- [7] W. Ma, S. Wei, B. Zhang, W. Li, Molecular mechanisms of cardiomyocyte death in drug-induced cardiotoxicity, *Front. Cell Dev. Biol.* 8 (2020), 434, <https://doi.org/10.3389/fcell.2020.00434>.
- [8] E. Christidi, L.R. Brunham, Regulated cell death pathways in doxorubicin-induced cardiotoxicity, *Cell Death Dis.* 12 (2021), 339, <https://doi.org/10.1038/s41419-021-03614-x>.
- [9] D. Tang, R. Kang, T.V. Berghe, P. Vandenabeele, G. Kroemer, The molecular machinery of regulated cell death, *Cell Res.* 29 (2019) 347–364, <https://doi.org/10.1038/s41422-019-0164-5>.
- [10] L. Galluzzi, I. Vitale, S.A. Aaronson, J.M. Abrams, D. Adam, P. Agostinis, et al., Molecular mechanisms of cell death: recommendations of the nomenclature committee on cell death 2018, *Cell Death Differ.* 25 (2018) 486–541, <https://doi.org/10.1038/s41418-017-0012-4>.
- [11] H. He, L. Wang, Y. Qiao, Q. Zhou, H. Li, S. Chen, et al., Doxorubicin induces endotheliotoxicity and mitochondrial dysfunction via ROS/eNOS/NO pathway, *Front. Pharmacol.* 10 (2020), 1531, <https://doi.org/10.3389/fphar.2019.01531>.
- [12] W. Wu, B. Yang, Y. Qiao, Q. Zhou, H. He, M. He, Kaempferol protects mitochondria and alleviates damages against endotheliotoxicity induced by doxorubicin, *Biomed. Pharmacother.* 126 (2020), 110040, <https://doi.org/10.1016/j.biopha.2020.110040>.
- [13] B. Yang, H. Li, Y. Qiao, Q. Zhou, S. Chen, D. Yin, et al., Tetramethylpyrazine attenuates the endotheliotoxicity and the mitochondrial dysfunction by doxorubicin via 14-3-3 γ /Bcl-2, *Oxid. Med. Cell Longev.* (2019), 5820415, <https://doi.org/10.1155/2019/5820415>, 2019.
- [14] X. Chen, X. Peng, Y. Luo, J. You, D. Yin, Q. Xu, et al., Quercetin protects cardiomyocytes against doxorubicin-induced toxicity by suppressing oxidative stress and improving mitochondrial function via 14-3-3 γ , *Toxicol. Mech. Methods* 29 (2019) 344–354, <https://doi.org/10.1080/15376516.2018.1564948>.
- [15] H. He, Y. Luo, Y. Qiao, Z. Zhang, D. Yin, J. Yao, et al., Curcumin attenuates doxorubicin-induced cardiotoxicity via suppressing oxidative stress and preventing mitochondrial dysfunction mediated by 14-3-3 γ , *Food Funct.* 9 (2018) 4404–4418, <https://doi.org/10.1039/C8FO00466H>.
- [16] D.L. Li, Z.V. Wang, G. Ding, W. Tan, X. Luo, A. Criollo, et al., Doxorubicin blocks cardiomyocyte autophagic flux by inhibiting lysosome acidification, *Circulation* 133 (2016) 1668–1687, <https://doi.org/10.1161/CIRCULATIONAHA.115.017443>.
- [17] S.Y. Yu, L. Liu, P. Li, J. Li, Rapamycin inhibits the mTOR/p70S6K pathway and attenuates cardiac fibrosis in adriamycin-induced dilated cardiomyopathy, *Thorac. Cardiovasc. Surg.* 61 (2013) 223–228, <https://doi.org/10.1055/s-0032-1311548>.
- [18] J.H. Park, S.H. Choi, H. Kim, S.T. Ji, W.B. Jang, J.H. Kim, et al., Doxorubicin regulates autophagy signals via accumulation of cytosolic Ca²⁺ in human cardiac progenitor cells, *Int. J. Mol. Sci.* 17 (2016), 1680, <https://doi.org/10.3390/ijms17101680>.
- [19] X. Fang, H. Wang, D. Han, E. Xie, X. Yang, J. Wei, et al., Ferroptosis as a target for protection against cardiomyopathy, *Proc. Natl. Acad. Sci. U. S. A.* 116 (2019) 2672–2680, <https://doi.org/10.1073/pnas.1821022116>.

- [20] Y. Liu, L. Zeng, Y. Yang, C. Chen, D. Wang, H. Wang, Acyl-CoA thioesterase 1 prevents cardiomyocytes from Doxorubicin-induced ferroptosis via shaping the lipid composition, *Cell Death Dis.* 11 (2020), 756, <https://doi.org/10.1038/s41419-020-02948-2>.
- [21] T. Tadokoro, M. Ikeda, T. Ide, H. Deguchi, S. Ikeda, K. Okabe, et al., Mitochondria-dependent ferroptosis plays a pivotal role in doxorubicin cardiotoxicity, *JCI Insight* 5 (2020), e132747, <https://doi.org/10.1172/jci.insight.132747>.
- [22] X. Jiang, B.R. Stockwell, M. Conrad, Ferroptosis: mechanisms, biology and role in disease, *Nat. Rev. Mol. Cell Biol.* 22 (2021) 266–282, <https://doi.org/10.1038/s41580-020-00324-8>.
- [23] N. Li, W. Jiang, W. Wang, R. Xiong, X. Wu, Q. Geng, Ferroptosis and its emerging roles in cardiovascular diseases, *Pharmacol. Res.* 166 (2021), 105466, <https://doi.org/10.1016/j.phrs.2021.105466>.
- [24] Q.Y. Eng, P.V. Thanikachalam, S. Ramamurthy, Molecular understanding of Epigallocatechin gallate (EGCG) in cardiovascular and metabolic diseases, *J. Ethnopharmacol.* 210 (2018) 296–310, <https://doi.org/10.1016/j.jep.2017.08.035>.
- [25] L. Xing, H. Zhang, R. Qi, R. Tsao, Y. Mine, Recent advances in the understanding of the health benefits and molecular mechanisms associated with green tea polyphenols, *J. Agric. Food Chem.* 67 (2019) 1029–1043, <https://doi.org/10.1021/acs.jafc.8b06146>.
- [26] P. Koonyosying, S. Kongkarnka, C. Uthaiyibull, S. Svasti, S. Fucharoen, S. Srichairatanakool, Green tea extract modulates oxidative tissue injury in beta-thalassemic mice by chelation of redox iron and inhibition of lipid peroxidation, *Biomed. Pharmacother.* 108 (2018) 1694–1702, <https://doi.org/10.1016/j.biopha.2018.10.017>.
- [27] J. Zhao, L. Xu, Q. Liang, Q. Sun, C. Chen, Y. Zhang, et al., Metal chelator EGCG attenuates Fe(III)-induced conformational transition of α -synuclein and protects AS-PC12 cells against Fe(III)-induced death, *J. Neurochem.* 143 (2017) 136–146, <https://doi.org/10.1111/jnc.14142>.
- [28] H. Ding, Y. Li, W. Li, H. Tao, L. Liu, C. Zhang, et al., Epigallocatechin-3-gallate activates the AMP-activated protein kinase signaling pathway to reduce lipid accumulation in canine hepatocytes, *J. Cell. Physiol.* 236 (2021) 405–416, <https://doi.org/10.1038/s41419-020-02948-2>.
- [29] L.G. Xiong, Y.J. Chen, J.W. Tong, Y.S. Gong, J.A. Huang, Z.H. Liu, Epigallocatechin-3-gallate promotes healthy lifespan through mitohormesis during early-to-mid adulthood in *Caenorhabditis elegans*, *Redox Biol.* 14 (2018) 305–315, <https://doi.org/10.1016/j.redox.2017.09.019>.
- [30] J. Lu, B. Fang, Y. Huang, S. Tao, B. Sun, S. Guan, et al., Epigallocatechin-3-gallate protects against 1,3-dichloro-2-propanol-induced lipid accumulation in C57BL/6J mice, *Life Sci.* 209 (2018) 324–331, <https://doi.org/10.1016/j.lfs.2018.08.007>.
- [31] W. Li, S. Nie, M. Xie, Y. Chen, C. Li, H. Zhang, A major green tea component, (-)-epigallocatechin-3-gallate, ameliorates doxorubicin-mediated cardiotoxicity in cardiomyocytes of neonatal rats, *J. Agric. Food Chem.* 58 (2010) 8977–8982, <https://doi.org/10.1021/jf101277t>.
- [32] Y.F. Yao, X. Liu, W.J. Li, Z.W. Shi, Y.X. Yan, L.F. Wang, et al., (-)-Epigallocatechin-3-gallate alleviates doxorubicin-induced cardiotoxicity in sarcoma 180 tumor-bearing mice, *Life Sci.* 180 (2017) 151–159, <https://doi.org/10.1016/j.lfs.2016.12.004>.
- [33] W. Li, S. Nie, M. Xie, Y. Chen, C. Li, H. Zhang, A major green tea component, (-)-epigallocatechin-3-gallate, ameliorates doxorubicin-mediated cardiotoxicity in cardiomyocytes of neonatal rats, *J. Agric. Food Chem.* 58 (2010) 8977–8982, <https://doi.org/10.1021/jf101277t>.
- [34] L.W. Xie, S. Cai, T.S. Zhao, M. Li, Y. Tian, Green tea derivative (-)-epigallocatechin-3-gallate (EGCG) confers protection against ionizing radiation-induced intestinal epithelial cell death both in vitro and in vivo, *Free Radic. Biol. Med.* 161 (2020) 175–186, <https://doi.org/10.1016/j.freeradbiomed.2020.10.012>.
- [35] T. Kose, M. Vera-Aviles, P.A. Sharp, G.O. Latunde-Dada, Curcumin and (-)-epigallocatechin-3-gallate protect murine MIN6 pancreatic beta-cells against iron toxicity and erastin-induced ferroptosis, *Pharmaceuticals* 12 (2019) 26, <https://doi.org/10.3390/ph12010026>.
- [36] J. Wang, Y. Chen, L. Chen, Y. Duan, X. Kuang, Z. Peng, et al., EGCG modulates PKD1 and ferroptosis to promote recovery in ST rats, *Transl. Neurosci.* 11 (2020) 173–181, <https://doi.org/10.1515/tnsci-2020-0119>.
- [37] Y. Qiao, T. Hu, B. Yang, H. Li, T. Chen, D. Yin, et al., Capsaicin alleviates the deteriorative mitochondrial function by upregulating 14-3-3 η in anoxic or anoxic/reoxygenated cardiomyocytes, *Oxid. Med. Cell Longev.* 2020 (2020), 1750289, <https://doi.org/10.1155/2020/1750289>.
- [38] Y. Qiao, T. Hu, B. Yang, H. Li, T. Chen, D. Yin, et al., Capsaicin alleviates the deteriorative mitochondrial function by upregulating 14-3-3 η in anoxic or anoxic/reoxygenated cardiomyocytes, *Oxid. Med. Cell Longev.* 2020 (2020), 1750289, <https://doi.org/10.1155/2020/1750289>.
- [39] D. Shin, E.H. Kim, J. Lee, J.L. Roh, RITA plus 3-MA overcomes chemoresistance of head and neck cancer cells via dual inhibition of autophagy and antioxidant systems, *Redox Biol.* 13 (2017) 219–227, <https://doi.org/10.1016/j.redox.2017.05.025>.
- [40] J. Zhang, Q. Wang, C. Xu, Y. Lu, H. Hu, B. Qin, et al., MitoTEMPO prevents oxalate induced injury in NRK-52E cells via inhibiting mitochondrial dysfunction and modulating oxidative stress, *Oxid. Med. Cell Longev.* (2017), 7528090, <https://doi.org/10.1155/2017/7528090>.
- [41] D. Liu, Z. Ma, S. Di, Y. Yang, J. Yang, L. Xu, et al., AMPK/GPC1 α activation by melatonin attenuates acute doxorubicin cardiotoxicity via alleviating mitochondrial oxidative damage and apoptosis, *Free Radic. Biol. Med.* 129 (2018) 59–72, <https://doi.org/10.1016/j.freeradbiomed.2018.08.032>.
- [42] S.Y. Yu, B. Dong, Z.F. Fang, X.Q. Hu, L. Tang, S.H. Zhou, Knockdown of lncRNA AK139328 alleviates myocardial ischaemia/reperfusion injury in diabetic mice via modulating miR-204-3p and inhibiting autophagy, *J. Cell Mol. Med.* 22 (2018) 4886–4898, <https://doi.org/10.1111/jcmm.13754>.
- [43] Z. Zhang, M. Guo, Y. Li, M. Shen, D. Kong, J. Shao, et al., RNA-binding protein ZFP36/TTP protects against ferroptosis by regulating autophagy signaling pathway in hepatic stellate cells, *Autophagy* 16 (2020) 1482–1505, <https://doi.org/10.1080/15548627.2019.1687985>.
- [44] P. Liu, D. Wu, J. Duan, H. Xiao, Y. Zhou, L. Zhao, et al., NRF2 regulates the sensitivity of human NSCLC cells to cystine deprivation-induced ferroptosis via FOCAD-FAK signaling pathway, *Redox Biol.* 37 (2020), 101702, <https://doi.org/10.1016/j.redox.2020.101702>.
- [45] C. Ge, L. Hu, D. Lou, Q. Li, J. Feng, Y. Wu, et al., Nr2f2 deficiency aggravates PM_{2.5}-induced cardiomyopathy by enhancing oxidative stress, fibrosis and inflammation via RIPK3-regulated mitochondrial disorder, *Aging (N Y)* 12 (2020) 4836–4865, <https://doi.org/10.18632/aging.102906>.
- [46] W. Flameng, M. Borgers, W. Daenen, G. Stalpaert, Ultrastructural and cytochemical correlates of myocardial protection by cardiac hypothermia in man, *J. Thorac. Cardiovasc. Surg.* 79 (1980) 413–424. PMID: 6243726.
- [47] K. Ito, Y. Eguchi, Y. Imagawa, S. Akai, H. Mochizuki, Y. Tsujimoto, MPP+ induces necrostatin-1- and ferrostatin-1-sensitive necrotic death of neuronal SH-SY5Y cells, *Cell Death Discov.* 3 (2017), 17013, <https://doi.org/10.1038/cddiscovery.2017.13>.
- [48] E. Jirkovský, A. Jirkovská, J. Bureš, J. Chládek, O. Lenčová, J. Stariat, et al., Pharmacokinetics of the cardioprotective drug dexrazoxane and its active metabolite ADR-925 with focus on cardiomyocytes and the heart, *J. Pharmacol. Exp. Therapeut.* 364 (2018) 433–446, <https://doi.org/10.1124/jpet.117.244848>.
- [49] E.C. Thomas, S.C. Hook, A. Gray, A. Chadt, D. Carling, H. Al-Hasani, et al., Isoform-specific AMPK association with TBC1D1 is reduced by a mutation associated with severe obesity, *Biochem. J.* 475 (2018) 2969–2983, <https://doi.org/10.1042/BCJ20180475>.
- [50] Y. Zong, C.S. Zhang, M. Li, W. Wang, Z. Wang, S.A. Hawley, et al., Hierarchical activation of compartmentalized pools of AMPK depends on severity of nutrient or energy stress, *Cell Res.* 29 (2019) 460–473, <https://doi.org/10.1038/s41422-019-0163-6>.
- [51] Z. Cai, C.F. Li, F. Han, C. Liu, A. Zhang, C.C. Hsu, et al., Phosphorylation of PDHA by AMPK drives TCA cycle to promote cancer metastasis, *Mol. Cell* 80 (2020) 263–278, <https://doi.org/10.1016/j.molcel.2020.09.018>.
- [52] N. Koleini, B.E. Nickel, A.L. Edel, R.R. Fandrich, A. Ravandi, E. Kardami, Oxidized phospholipids in Doxorubicin-induced cardiotoxicity, *Chem. Biol. Interact.* 303 (2019) 35–39, <https://doi.org/10.1016/j.cbi.2019.01.032>.
- [53] G. Takemura, H. Fujiwara, Doxorubicin-induced cardiomyopathy from the cardiotoxic mechanisms to management, *Prog. Cardiovasc. Dis.* 49 (2007) 330–352, <https://doi.org/10.1016/j.pcad.2006.10.002>.
- [54] A. Varela-López, M. Battino, M.D. Navarro-Hortal, F. Giampieri, T.Y. Forbes-Hernández, J.M. Romero-Márquez, et al., An update on the mechanisms related to cell death and toxicity of doxorubicin and the protective role of nutrients, *Food Chem. Toxicol.* 134 (2019), 110834, <https://doi.org/10.1016/j.fct.2019.110834>.
- [55] A.R. Coelho, T.R. Martins, R. Couto, C. Deus, C.V. Pereira, R.F. Simões, et al., Berberine-induced cardioprotection and Sirt3 modulation in doxorubicin-treated H9c2 cardiomyoblasts, *Biochim. Biophys. Acta (BBA) - Mol. Basis Dis.* 1863 (2017) 2904–2923, <https://doi.org/10.1016/j.bbadis.2017.07.030>.
- [56] X. Lv, X. Yu, Y. Wang, F. Wang, H. Li, Y. Wang, et al., Berberine inhibits doxorubicin-triggered cardiomyocyte apoptosis via attenuating mitochondrial dysfunction and increasing Bcl-2 expression, *PLoS One* 7 (2012), e47351, <https://doi.org/10.1371/journal.pone.0047351>.
- [57] Y.Z. Wu, L. Zhang, Z.X. Wu, T.T. Shan, C. Xiong, Berberine ameliorates doxorubicin-induced cardiotoxicity via a SIRT1/p66Shc-mediated pathway, *Oxid. Med. Cell Longev.* (2019), 2150394, <https://doi.org/10.1155/2019/2150394>.
- [58] D.A. Stoyanovsky, Y.Y. Tyurina, I. Shrivastava, I. Bahar, V.A. Tyurin, O. Protchenko, et al., Iron catalysis of lipid peroxidation in ferroptosis: regulated enzymatic or random free radical reaction? *Free Radic. Biol. Med.* 133 (2019) 153–161, <https://doi.org/10.1016/j.freeradbiomed.2018.09.008>.
- [59] S. Deng, T. Yan, C. Jendry, A. Nemecek, M. Vincetic, U. Gödtel-Armbust, et al., Dexrazoxane may prevent doxorubicin-induced DNA damage via depleting both topoisomerase II isoforms, *BMC Cancer* 14 (2014), 842, <https://doi.org/10.1186/1471-2407-14-842>.
- [60] T. Ha, M.K. Kim, K.S. Park, W. Jung, H. Choo, Y. Chong, Structural modification of (-)-Epigallocatechin gallate (EGCG) shows significant enhancement in mitochondrial biogenesis, *J. Agric. Food Chem.* 66 (2018) 3850–3859, <https://doi.org/10.1021/acs.jafc.8b00364>.
- [61] F. Li, C. Gao, P. Yan, M. Zhang, Y. Wang, Y. Hu, et al., EGCG reduces obesity and white adipose tissue gain partly through AMPK activation in mice, *Front. Pharmacol.* 9 (2018), 1366, <https://doi.org/10.3389/fphar.2018.01366>.
- [62] X. Li, Y. Chen, J.Z. Shen, Q. Pan, W. Yang, H. Yan, et al., Epigallocatechin gallate inhibits hepatic glucose production in primary hepatocytes via downregulating PKA signaling pathways and transcriptional factor FoxO1, *J. Agric. Food Chem.* 67 (2019) 3651–3661, <https://doi.org/10.1021/acs.jafc.9b00395>.
- [63] C. Chen, Q. Liu, L. Liu, Y.Y. Hu, Q. Feng, Potential biological effects of (-)-Epigallocatechin-3-gallate on the treatment of nonalcoholic fatty liver disease, *Mol. Nutr. Food Res.* 62 (2018), 1700483, <https://doi.org/10.1002/mnfr.201700483>.
- [64] M. Holczer, B. Besze, V. Zámbo, M. Csala, G. Bánhegyi, O. Kapuy, Epigallocatechin-3-Gallate (EGCG) promotes autophagy-dependent survival via influencing the

- balance of mTOR-AMPK pathways upon endoplasmic reticulum stress, *Oxid. Med. Cell Longev.* (2018), 6721530, <https://doi.org/10.1155/2018/6721530>, 2018.
- [65] H.S. Kim, V. Montana, H.J. Jang, V. Parpura, J.A. Kim, Epigallocatechin gallate (EGCG) stimulates autophagy in vascular endothelial cells: a potential role for reducing lipid accumulation, *J. Biol. Chem.* 288 (2013) 22693–22705, <https://doi.org/10.1074/jbc.M113.477505>.
- [66] D.J. Klionsky, K. Abdelmohsen, A. Abe, M.J. Abedin, H. Abeliovich, A. Acevedo Arozana, et al., Guidelines for the use and interpretation of assays for monitoring autophagy, *Autophagy* 12 (2016) 1–222, <https://doi.org/10.1080/15548627.2015.1100356>, third ed.
- [67] F. Giampieri, S. Afrin, T.Y. Forbes-Hernandez, M. Gasparrini, D. Cianciosi, P. Reboredo-Rodriguez, et al., Autophagy in human health and disease: novel therapeutic opportunities, *Antioxidants Redox Signal.* 30 (2019) 577–634, <https://doi.org/10.1089/ars.2017.7234>.
- [68] D. Dutta, J. Xu, M.L. Dirain, C. Leeuwenburgh, Calorie restriction combined with resveratrol induces autophagy and protects 26-month-old rat hearts from doxorubicin-induced toxicity, *Free Radic. Biol. Med.* 74 (2014) 252–262, <https://doi.org/10.1016/j.freeradbiomed.2014.06.011>.
- [69] S.E. Hall, A.J. Smuder, R. Hayward, Effects of calorie restriction and voluntary exercise on doxorubicin-induced cardiotoxicity, *Integr. Cancer Ther.* 18 (2019), 1534735419843999, <https://doi.org/10.1177/1534735419843999>.
- [70] T. Kawaguchi, G. Takemura, H. Kanamori, T. Takeyama, T. Watanabe, K. Morishita, et al., Prior starvation mitigates acute doxorubicin cardiotoxicity through restoration of autophagy in affected cardiomyocytes, *Cardiovasc. Res.* 96 (2012) 456–465, <https://doi.org/10.1093/cvr/cvs282>.
- [71] M.S. Mitra, S. Donthamsetty, B. White, J.R. Latendresse, H.M. Mehendale, Mechanism of protection of moderately diet restricted rats against doxorubicin-induced acute cardiotoxicity, *Toxicol. Appl. Pharmacol.* 225 (2007) 90–101, <https://doi.org/10.1016/j.taap.2007.07.018>.
- [72] X. Xu, J. Pang, Y. Chen, R. Bucala, Y. Zhang, J. Ren, Macrophage migration inhibitory factor (MIF) deficiency exacerbates aging-induced cardiac remodeling and dysfunction despite improved inflammation: role of autophagy regulation, *Sci. Rep.* 6 (2016), 22488, <https://doi.org/10.1038/srep22488>.
- [73] P. Wang, M. Wang, Y. Hu, J. Chen, Y. Cao, C. Liu, et al., Isorhapontigenin protects against doxorubicin-induced cardiotoxicity via increasing YAP1 expression, *Acta Pharm. Sin. B* 11 (2021) 680–693, <https://doi.org/10.1016/j.apsb.2020.10.017>.
- [74] P. Xia, J. Chen, Y. Liu, M. Fletcher, B.C. Jensen, Z. Cheng, Doxorubicin induces cardiomyocyte apoptosis and atrophy through cyclin-dependent kinase 2-mediated activation of forkhead box O1, *J. Biol. Chem.* 295 (2020) 4265–4276, <https://doi.org/10.1074/jbc.RA119.011571>.
- [75] P. Wang, R. Lan, Z. Guo, S. Cai, J. Wang, Q. Wang, et al., Histone demethylase JMJD3 mediated doxorubicin-induced cardiomyopathy by suppressing SESN2 expression, *Front. Cell Dev. Biol.* 8 (2020), 548605, <https://doi.org/10.3389/fcell.2020.548605>.
- [76] X. Liang, S. Wang, L. Wang, A.F. Ceylan, J. Ren, Y. Zhang, Mitophagy inhibitor liensinine suppresses doxorubicin-induced cardiotoxicity through inhibition of Drp1-mediated maladaptive mitochondrial fission, *Pharmacol. Res.* 157 (2020), 104846, <https://doi.org/10.1016/j.phrs.2020.104846>.